



Geochronology and geochemistry of the Paleoproterozoic Fe-rich mafic sills from the Zhongtiao Mountains: Petrogenesis and tectonic implications



Ning-Bo Li^{a,b}, He-Cai Niu^{a,*}, Zhi-Wei Bao^a, Qiang Shan^a, Wu-Bin Yang^a, Yu-Hang Jiang^{a,b}, Ling-Jun Zeng^{a,b}

^a CAS Key Laboratory of Mineralogy and Metallogeny, Guangzhou Institute of Geochemistry, Chinese Academy of Sciences, Guangzhou 510640, China

^b University of Chinese Academy of Sciences, Beijing 100049, China

ARTICLE INFO

Article history:

Received 29 October 2013

Received in revised form 10 August 2014

Accepted 30 August 2014

Available online 28 September 2014

Keywords:

Fe-rich mafic sills

Mantle wedge

Back-arc basin

Zhongtiao Mountains (ZTM)

Trans-North China Orogen (TNCO)

ABSTRACT

Despite the existence of the Trans-North China Orogen (TNCO) in the middle part of the North China Craton (NCC) is widely accepted, its formation timing and mechanism are still controversial. A suite of Paleoproterozoic Fe-rich mafic sills in the Zhongtiao Mountains (ZTM) in the southern TNCO has been investigated to constrain the formation of the TNCO. Our new zircon U-Pb dating on these sills has yielded a Paleoproterozoic age of 1897 ± 30 Ma, and our new geochemical data have suggested an arc-affinity with significant Nb, Ta and Ti depletions. Geochemical evidence further reveals that the mantle source of the ZTM Fe-rich mafic sills was mainly composed of spinel lherzolite, and may have been metasomatized by reduced subduction-related fluids. With these age and geochemical data, we propose a genetic model for the ZTM Fe-rich mafic sills: (1) Subduction-related fluids may have transported Fe from the subducted plate and the overlying mantle wedge to generate the Fe-enriched source at the upper part of mantle wedge; (2) Partial melting of the Fe-enriched source may have generated the primary magmas of the Fe-rich mafic sills, which has evolved under a low oxygen fugacity (FO_2) condition and eventually formed the Fe-rich mafic sills. The ZTM Fe-rich mafic sills have moderate Ti/V values (28–36) and La/Nb values (2.3–3.3), suggesting that they may have formed in a back-arc setting. The existence of a back-arc basin at ~ 1900 Ma in the ZTM indicates that the TNCO was formed during the ~ 1850 Ma final collision between the Western- and Eastern blocks of the NCC.

© 2014 Elsevier B.V. All rights reserved.

1. Introduction

The North China Craton (NCC), one of world's oldest cratons (Liu et al., 1992, 2007, 2008; Song et al., 1996; Wan et al., 2012), has undergone a long and complex structural and thermal evolution history, especially in the Precambrian (Santosh, 2010; Zhai, 2010; Kusky, 2011; Zhai and Santosh, 2011, 2013; Wan et al., 2011; Zhao and Zhai, 2013). Although the 2600–2500 Ma rocks have accounted for $\sim 80\%$ of the Precambrian NCC basement, whole-rock Nd and zircon Hf model ages have revealed that these rocks were mainly formed through the reworking of 2800–2700 Ma crustal rocks (Zhao and Zhai, 2013 and references therein). The recognition of the Trans-North China Orogen (TNCO) has led to the general agreement that the NCC has been formed by the amalgamation of

two continental blocks, namely Eastern- (or Yanliao) and Western blocks (Fig. 1a, Zhao et al., 2001, 2005, 2010; Kusky and Li, 2003; Kröner et al., 2005; Wilde and Zhao, 2005; Li et al., 2011; Liu et al., 2012). Nevertheless, the subduction polarity and the final collision timing between these two blocks are still controversial (Zhai and Santosh, 2011 and references therein). Various tectonic models have been proposed for the TNCO formation:

- (1) Eastward subduction of an old oceanic plate followed by a continental collision at ~ 1850 Ma. This model is supported by detrital zircon U-Pb dating on sedimentary strata (Li et al., 2011; Liu et al., 2011a,b, 2012) and metamorphic zircon U-Pb ages (~ 1850 Ma) (Guan et al., 2002; Zhao et al., 2002, 2008; Kröner et al., 2006; Zhang et al., 2009).
- (2) Westward subduction with two Paleoproterozoic collisions at ~ 2100 and ~ 1850 Ma, with the latter one accounts for the main structural, metamorphic and magmatic features of the TNCO. This model is supported by the polyphase deformation and

* Corresponding author. Tel.: +86 20 85290906; fax: +86 20 85290130.
E-mail address: niuhc@gig.ac.cn (H.-C. Niu).

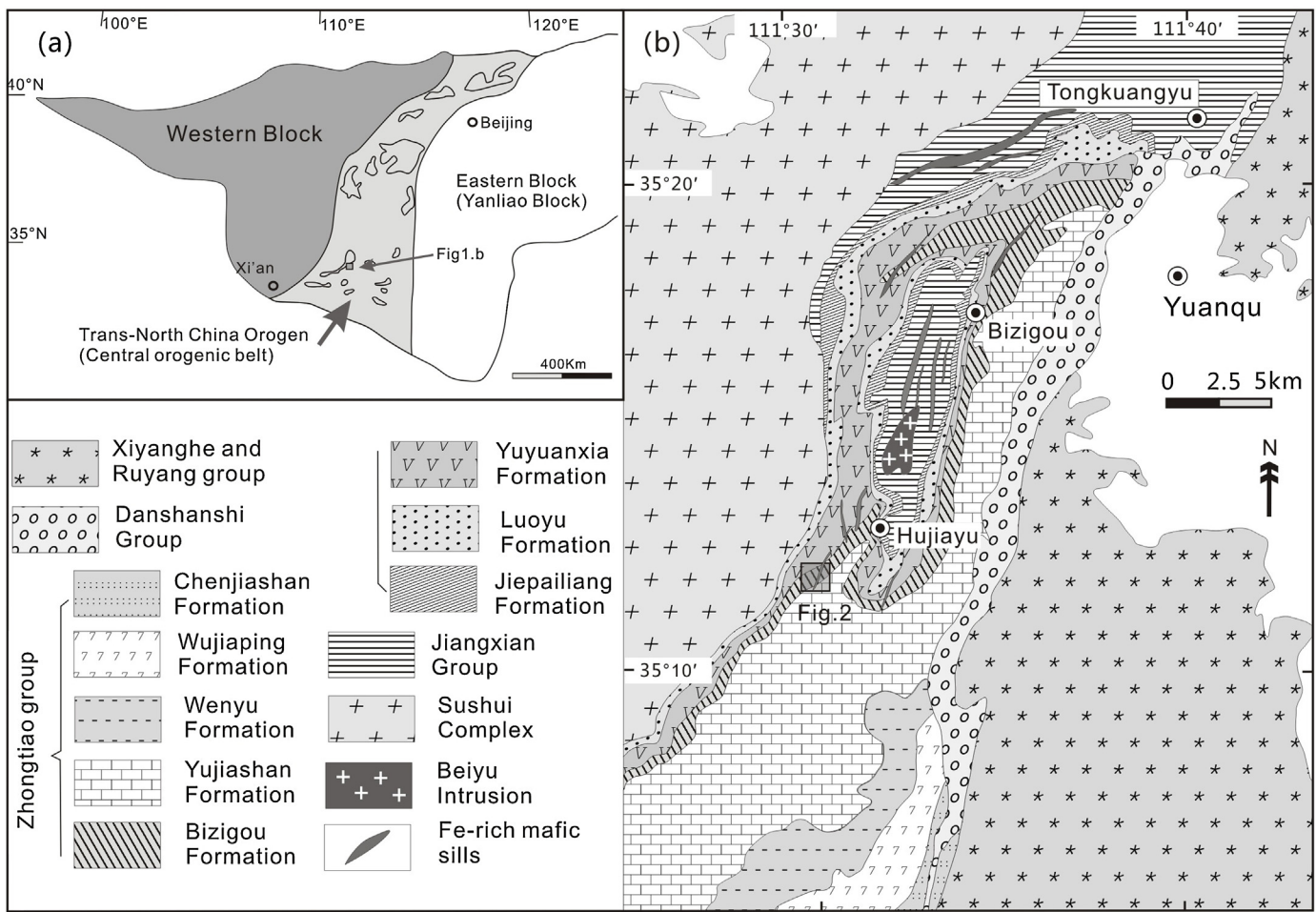


Fig. 1. (a) Tectonic subdivision of the North China Craton and location of the Zhongtiao Mountains (after Zhao et al., 2005); and (b) simplified geological map of the Zhongtiao Mountains (after Sun and Hu, 1993).

- abundant ~2100 Ma granitoids (Faure et al., 2007; Trap et al., 2007, 2008).
- (3) Westward subduction with the final collision occurred at ~2500 Ma, and the ~1850 Ma metamorphic events may have corresponded to the Columbia supercontinent assembly (Kusky and Li, 2003; Kusky et al., 2007a,b). This model is supported by the questionable existence of a foreland basin on the Eastern Block and seismic imaging across the TNCO (Kusky and Li, 2003; Kusky et al., 2007a,b; Kusky, 2011; Zheng et al., 2009).
 - (4) Several micro-blocks being amalgamated at ~2500 Ma. The amalgamated block may have undergone rifting at ~2100 Ma. Rift basins may have evolved into ocean basins, followed by subduction and eventually by continent-continent collisions during 1970–1820 Ma (Zhai et al., 2010; Zhai and Santosh, 2013; Wang et al., 2014).

Tectonic evolution of the TNCO at 2500–1800 Ma, especially ~1850 Ma is very important for the formation of the NCC. Mafic dikes and sills are useful to constrain the regional tectonic setting due to they generally have a short life span and can preserve their original geochemical characteristics well (e.g., Wang et al., 2004, 2008, 2014; Peng et al., 2005, 2007, 2011; Hollings et al., 2010, 2012). Paleoproterozoic mafic dikes formed approach 1850 Ma in the TNCO are divided into strongly metamorphosed and weakly-/un-metamorphosed types. The weakly-/un-metamorphosed mafic dikes include the 1769 ± 3 Ma dolerite dike (Halls et al., 2000), the ~1770 Ma high Fe dikes (Wang

et al., 2004, 2008) and ~1780 Ma high Fe-Ti mafic dikes (Peng et al., 2007, 2005). The strongly metamorphosed mafic dikes include the ~1914 Ma mafic dikes in Dashiyan (Kröner et al., 2006) and the ~1940 Ma dikes in Lvliang (Wang et al., 2014). All the dike swarms mentioned above are distributed in the northern part of the TNCO and have been studied previously (e.g., Wang et al., 2004, 2014, 2008; Peng et al., 2005, 2007; Kröner et al., 2006). However, systematic research on the mafic dikes and sills in the southern part of the TNCO, especially the Zhongtiao Mountains (ZTM), is relatively limited.

The ZTM mafic dikes have been documented in some previous studies (e.g., Sun and Hu, 1993; Bai et al., 1997; Peng et al., 2007), yet detailed isotopic, geochemical and geochronologic analyses are still lacking. To investigate the petrogenesis of the ZTM Fe-rich mafic sills and delineate the regional Proterozoic geodynamic evolution, we have carried out comprehensive study on ZTM Fe-rich mafic sills, zircon U-Pb geochronology, whole rock and mineral geochemistry.

2. Regional geology and petrography

The TNCO (~1200 km long and 100–300 km wide) is nearly N-S-trending and cut across the middle part of the NCC (Fig. 1a). Basement of the TNCO comprises Neoproterozoic tonalite-trondhjemite-granodiorite (TTG) gneisses, metamorphosed sedimentary- and volcanic rocks, syn- to post-tectonic granites and mafic dikes and sills. Geochemical data

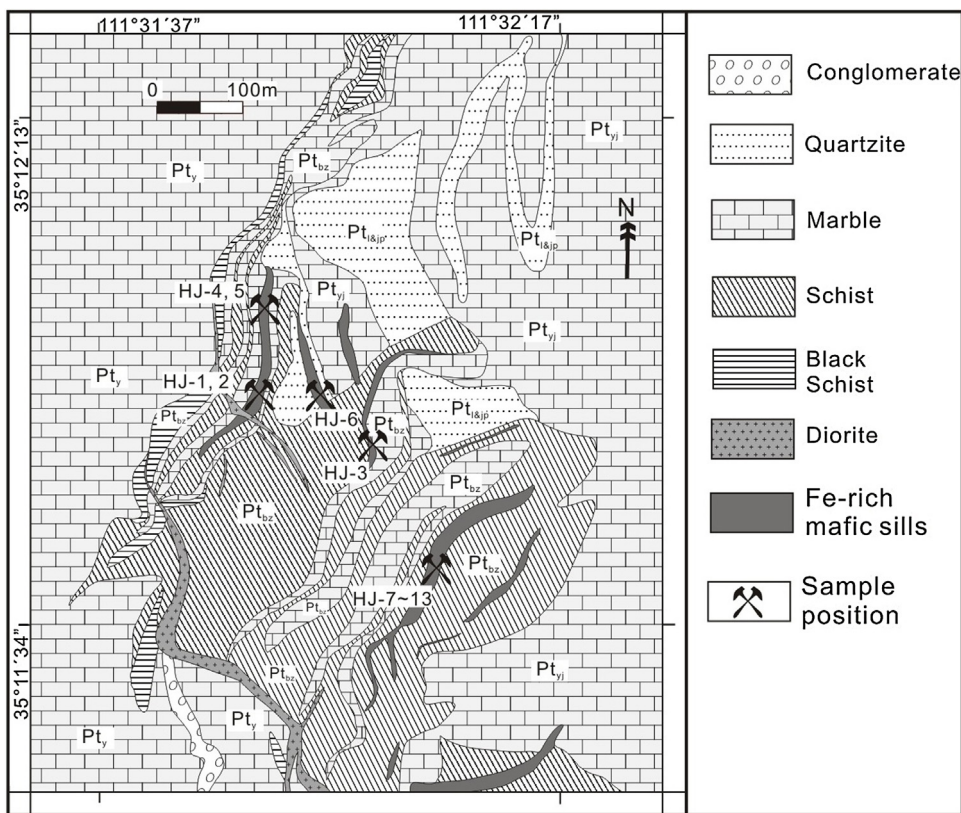


Fig. 2. Geological map and sample locations of the ZTM Fe-rich mafic sills. (Pt_{yj}: Yujiashan Formation; Pt_{l&jp}: Longyu and Jiepailing formations; Pt_{bz}: Bizigou Formation; Pt_y: Yuyuanxia Formation).

suggested that most of the basement rocks have been developed in subduction-related settings (Zhao and Zhai, 2013 and references therein). The ZTM is located in the southern segment of the TNCO. Similar to other parts of the TNCO, the ZTM contains extensive occurrence of Precambrian sedimentary strata and igneous rocks (Fig. 1b). The igneous rocks are of diverse compositions (from mafic to felsic) and ages (2500–1800 Ma) (Sun and Hu, 1993; Bai et al., 1997; Guo et al., 2008; Zhao et al., 2012; Li et al., 2013b), which make the ZTM an important region for studying the tectonic evolution of the NCC, and particularly of the TNCO. Regional Precambrian basement contains five tectonostratigraphic units as defined by unconformable contacts (Fig. 1b, Sun and Hu, 1993; Bai et al., 1997). From the oldest to the youngest, these tectonostratigraphic units are:

- (I) Sushui Complex is located in the western part of the ZTM and mainly consists of TTG gneiss. Sun and Hu (1993) suggested that the Sushui Complex has formed in Paleoproterozoic with some Archean remains. Recent studies have revealed that the complex may have mainly formed in two episodes, namely during ~2700 and ~2500 Ma (Yu et al., 2006; Zhao et al., 2012; Zhang et al., 2013a; Zhu et al., 2013), with local ~2600 Ma magmatism (Zhang et al., 2012a). The ~2700 Ma magmatism was synchronous with the main crustal growth phase of the NCC, whereas the ~2500 Ma magmatism may have represented a crustal reworking event in the NCC (Zhu et al., 2013).
- (II) Jiangxian Group is the host rock of the Tongkuangyu Cu deposit, which is the largest Cu deposit in the TNCO (Jiang et al., 2014). Sun et al. (1990) subdivided the Jiangxian Group into the Henglingguan and Tongkuangyu formations. The Henglingguan Formation consists mainly of clastic sediments, whereas the Tongkuangyu Formation consists of pyroclastic and volcanic

sedimentary rocks. The Tongkuangyu meta-tuffs give a zircon U–Pb age of 2155 Ma (Sun and Hu, 1993), whereas the detrital zircons from the Henglingguan Formation give a maximum deposition age of ~2170 Ma (Li et al., 2008). Based on Hf isotopic data of detrital zircons and whole-rock geochemical data for the metasedimentary rocks from the Jiangxian Group, Li et al. (2009) suggested that the Jiangxian Group was deposited in a back-arc basin in an active continental margin setting, but some other researchers proposed that the group was formed in a continental rift-related setting because of the existence of bimodal volcanic rocks (Sun and Hu, 1993; Zhai and Santosh, 2011).

- (III) Zhongtiao Group composed of eight formations and is generally subdivided into the Lower- and Upper Zhongtiao subgroups (Fig. 1b). The Lower Zhongtiao Subgroup is subdivided into five formations, namely Jiepailiang, Longyu, Yuyuanxia, Bizigou, and Yujiashan formations. Zircon U–Pb dating on the felsic volcanic rocks of the Bizigou Formation has yielded 2059 Ma (Sun and Hu, 1993). Li et al. (2011) and Liu et al. (2012) suggested that the Lower Zhongtiao Subgroup was deposited in a back-arc basin setting. The Upper Zhongtiao Subgroup is in a disconformable contact with the Lower Zhongtiao Group (Sun and Hu, 1993; Fig. 1b) and is subdivided into three formations, including Wenyu, Wujiaping and Chenjiashan formations. Detrital zircon U–Pb ages of the Chenjiashan Formation range from 1817 to 2477 Ma with a peak at ~2000 Ma. Liu et al. (2012, 2014) suggested that the Upper Zhongtiao Subgroup was deposited in a foreland basin setting.
- (IV) Danshansi Group is mainly composed of fluvial sedimentation and the deposition age is yet to be well constrained. Detrital zircon U–Pb ages range from 1900 to 3202 Ma, with two major peaks at ~2230 and ~2600 Ma. Sun and Hu (1993) suggested that the Danshansi Group is a typical molasse formation.

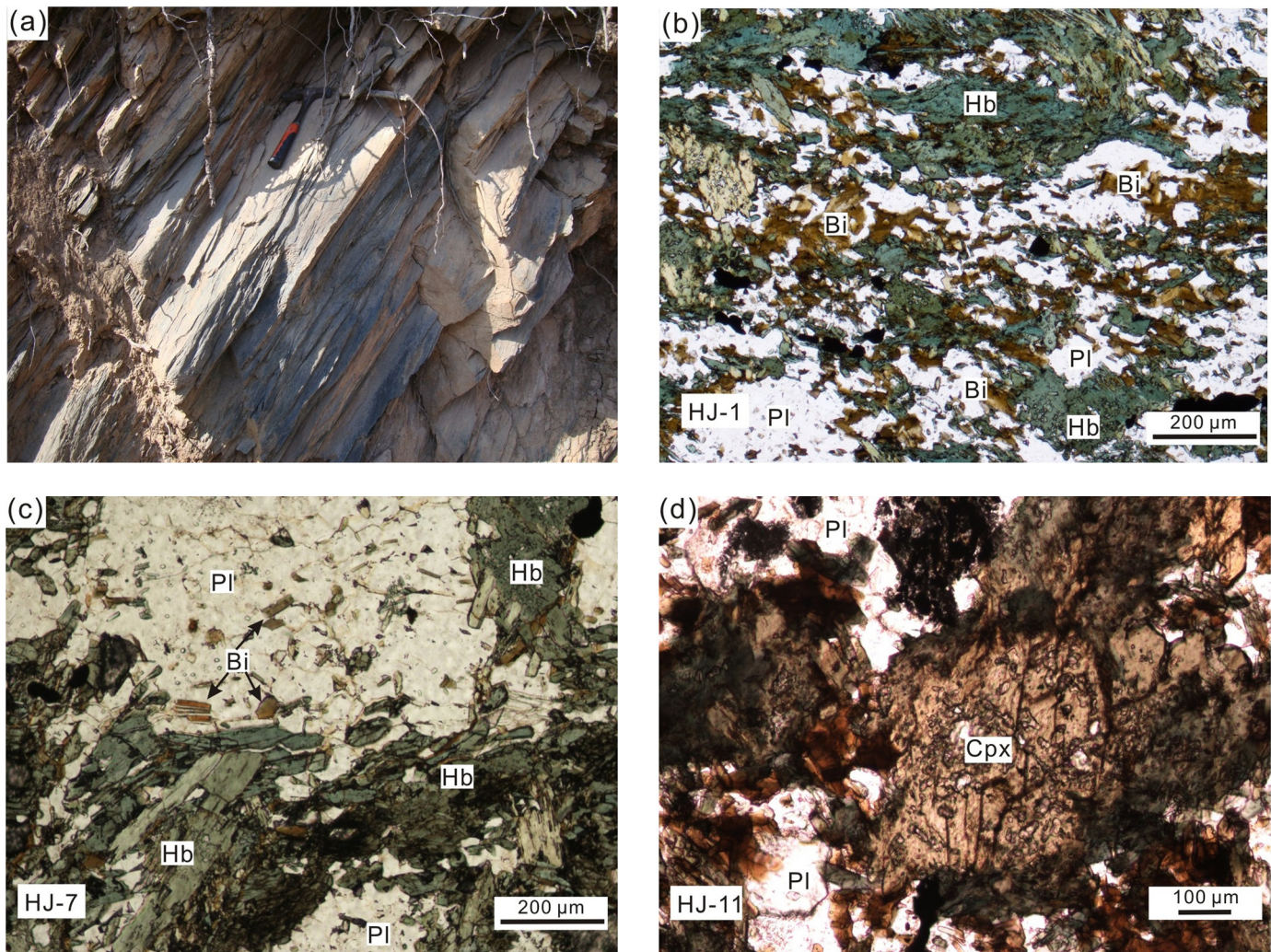


Fig. 3. Photographs of the ZTM Fe-rich mafic sills; (a) field photograph showing stretching lineation of the Fe-rich mafic sills; (b) optical micrograph of the Fe-rich mafic sill Sample HJ-1, showing biotite (Bi) clusters; (c) optical micrograph of the Fe-rich mafic sill Sample HJ-7, showing very few biotite (Bi); (d) Optical micrograph of the Fe-rich mafic sill Sample HJ-10, showing the presence of clinopyroxene (Cpx).

(V) Xiyanghe and Ruyang groups, which are considered to be the oldest sedimentary cover of the NCC, have a formation age of ~1830 Ma (Sun and Hu, 1993).

The ZTM Fe-rich mafic sills are roughly NE-trending and intruded mainly into the Lower Zhongtiao Subgroup and the Jiangxian Group (Figs. 1b and 2). In the study area, most of the Fe-rich mafic sills are intruded into the Bizigou Formation (Fig. 2), which is relatively complex due to a transitory regression and multiple magmatic overprinting. The Bizigou rocks have generally undergone low amphibolite-facies metamorphism (Sun and Hu, 1993; Bai et al., 1997). The ZTM Fe-rich mafic sills show obvious stretching lineation (Fig. 3a), and are composed of amphibole (40–50%), plagioclase (35–40%), magnetite (5–10%), biotite (1–5%) and minor quartz and clinopyroxene (Fig. 3).

3. Analytical methods

3.1. Zircon U–Pb dating

Zircon grains were separated from ~10 kg of ZTM Fe-rich mafic sills sample HJ-1 ($35^{\circ}11'53''$ N, $111^{\circ}31'57''$ E) using conventional density and magnetic separation techniques followed by

handpicking. Representative zircon separates were mounted in epoxy mounts, which were then polished to nearly half-section to expose internal structures. All mounted zircon were studied petrographically with transmitted and reflected light microscopy, as well as by cathodoluminescence (CL) imaging to reveal their internal structures.

Zircon U–Pb dating was performed on a laser ablation inductively coupled plasma spectrometry (LA-ICP-MS) at State Key Laboratory of Continental Dynamics of Northwest University. Zircon 91500 (Wiedenbeck et al., 1995) was used as the external standard for calibration. The analytical procedures were described by Yuan et al. (2004). Both isotope ratios and trace elements contents of zircon were calculated with the GLITTER 4.0 software (Macquarie University). Zircon ages were calculated with ISOPLOT 4.11 (Ludwig, 2008).

3.2. Major element compositions of amphiboles

Major element compositions of 28 amphiboles from the ZTM Fe-rich mafic sills were examined using a JEOL JXA 8800R electron microprobe (EMPA) at the Center of Instrumentation Analysis and Research in Sun Yat-sen University. The operating conditions are listed as follows: Accelerating voltage (15 kV), beam current

(20 nA), beam diameter ($1\text{ }\mu\text{m}$), with 30 s count times on peak and each background. All data were corrected with standard ZAF correction procedures. Natural minerals and synthetic glasses were used as the standards. The detailed procedure is described in Wang et al. (2009).

3.3. Whole-rock geochemical analyses

Major and trace element concentrations of 13 representative fresh or weakly altered ZTM Fe-rich mafic sills samples were analyzed at the State Key Laboratory of Isotope Geochemistry, Guangzhou Institute of Geochemistry Chinese Academy of Sciences (GIGCAS). Major elements were analyzed by the X-ray fluorescence (XRF) method following the procedures outlined by Li et al. (2005a). Trace elements were determined by using the Perkin-Elmer ELAN 6000 ICP-MS following procedures outlined by Li (1997), with less than 3% of standard deviations for most elements. Nd isotopic compositions were analyzed by using the Neptune Plus multi-collector (MC)-ICPMS at the GIGCAS, following procedures similar to those of Liang et al. (2003) and Li et al. (2005b). The mass fractionation corrections for Nd isotopic ratios were based on $^{143}\text{Nd}/^{144}\text{Nd}$ ratio of 0.7219. The $^{143}\text{Nd}/^{144}\text{Nd}$ ratio of the Standard Shin Etsu JNd-1 was determined to be 0.512115 ± 10 . Hf isotopic compositions were also analyzed by using the Neptune Plus MC-ICPMS at the GIGCAS, following procedures similar to those of Li et al. (2006). The $^{176}\text{Hf}/^{177}\text{Hf}$ ratios were normalized to $^{179}\text{Hf}/^{177}\text{Hf} = 0.7325$ using an exponential law for mass bias correction.

4. Results

4.1. Zircon U-Pb geochronology

Zircon grains from the ZTM Fe-rich mafic sills Sample HJ-1 were mostly transparent, colorless, well-developed prismatic crystals. CL imaging shows that these zircon grains have igneous oscillatory zoning with low luminescence (Fig. 4). 19 analysis spots give relatively high and widely varied Th/U ratios (1.48–3.44) (Table 1), which indicate a magmatic origin for these zircons (Yang et al., 2013). Most analyses were strongly discordant with an upper intercept age of 1905 ± 15 Ma, whereas three of the 19 analyses were plotted on or near the concordia and have yielded a weighted average $^{207}\text{Pb}/^{206}\text{Pb}$ age of 1897 ± 30 Ma (Fig. 4), consistent with the upper intercept age within errors. Thus, the 1897 ± 30 Ma age represents the crystallization age of the ZTM Fe-rich mafic sills.

Table 1
Zircon U-Pb isotopic results of the ZTM Fe-rich mafic sills.

Analysis	Ratios						Isotopic age (Ma)						
	Th/U	$^{207}\text{Pb}/^{206}\text{Pb}$	1σ	$^{207}\text{Pb}/^{235}\text{U}$	1σ	$^{206}\text{Pb}/^{238}\text{U}$	1σ	$^{207}\text{Pb}/^{206}\text{Pb}$	1σ	$^{206}\text{Pb}/^{238}\text{U}$	1σ	$^{207}\text{Pb}/^{235}\text{U}$	1σ
HJ-1@1	2.80	0.1106	0.0016	3.0120	0.0358	0.1975	0.0015	1809	26	1162	8	1411	9
HJ-1@2	2.80	0.1070	0.0014	2.3652	0.0259	0.1603	0.0012	1749	24	959	7	1232	8
HJ-1@3	2.63	0.1076	0.0015	2.5229	0.0281	0.1700	0.0013	1759	25	1012	7	1279	8
HJ-1@4	2.30	0.1129	0.0014	4.0408	0.0395	0.2595	0.0019	1847	22	1487	10	1643	8
HJ-1@5	3.29	0.1064	0.0014	2.3288	0.0253	0.1588	0.0012	1738	24	950	6	1221	8
HJ-1@6	1.73	0.1091	0.0015	2.7313	0.0308	0.1816	0.0014	1784	25	1076	7	1337	8
HJ-1@7	2.44	0.1137	0.0018	3.4805	0.0477	0.2220	0.0018	1859	28	1292	10	1523	11
HJ-1@8	2.34	0.1093	0.0014	3.2700	0.0349	0.2170	0.0016	1787	24	1266	8	1474	8
HJ-1@9	3.43	0.1046	0.0013	2.0365	0.0207	0.1412	0.0010	1708	23	851	6	1128	7
HJ-1@10	3.02	0.1070	0.0014	2.3602	0.0256	0.1599	0.0012	1750	24	956	7	1231	8
HJ-1@11	2.68	0.1062	0.0014	2.3746	0.0257	0.1622	0.0012	1735	24	969	7	1235	8
HJ-1@12	2.77	0.1148	0.0014	5.2285	0.0516	0.3304	0.0024	1877	22	1840	12	1857	8
HJ-1@13	2.32	0.1138	0.0017	3.9981	0.0510	0.2547	0.0020	1861	27	1463	10	1634	10
HJ-1@14	3.44	0.1043	0.0016	2.1988	0.0297	0.1529	0.0012	1702	28	917	7	1181	9
HJ-1@15	2.44	0.1174	0.0015	5.1250	0.0526	0.3165	0.0024	1918	22	1773	11	1840	9
HJ-1@16	1.48	0.1160	0.0034	5.1639	0.1446	0.3230	0.0043	1895	52	1805	21	1847	24
HJ-1@17	2.07	0.1134	0.0016	3.7112	0.0427	0.2374	0.0018	1854	25	1373	9	1574	9
HJ-1@18	3.13	0.1019	0.0016	2.0078	0.0265	0.1429	0.0011	1659	28	861	6	1118	9
HJ-1@19	3.43	0.1069	0.0015	2.4769	0.0283	0.1681	0.0013	1747	25	1002	7	1265	8

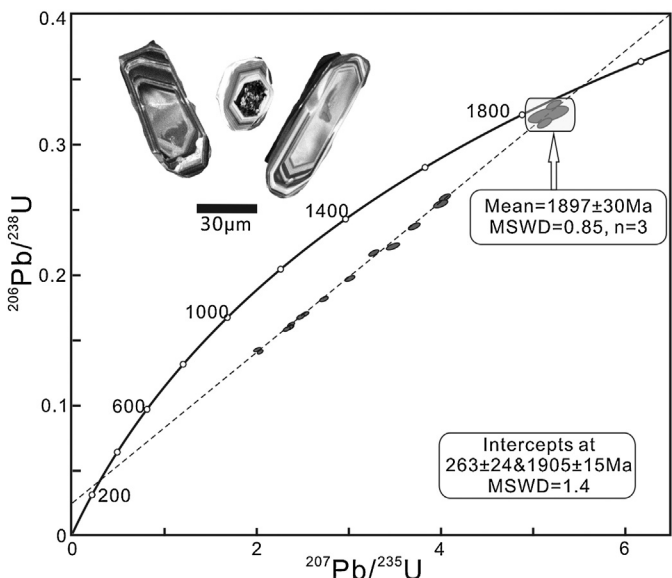


Fig. 4. Representative zircon CL images and concordia diagram for the ZTM Fe-rich mafic sills (sample HJ-1).

4.2. Mineral compositions

Amphiboles in the ZTM Fe-rich mafic sills have consistent geochemistry (Table 2), with low SiO_2 (38.33–45.71 wt.%), TiO_2 (0.60–0.78 wt.%), Na_2O (1.14–2.11 wt.%) and high FeO (22.44–24.81 wt.%) and Al_2O_3 (8.23–13.46 wt.%). All samples belong to Ca-amphiboles according to their $(\text{Ca} + \text{Na})_{\text{B}} > 1.0$, $\text{Na}_{\text{B}} < 0.50$ and $\text{Ca}_{\text{B}} > 1.50$ (Leake et al., 1997). The amphiboles have $\text{Mg}/(\text{Mg} + \text{Fe}^{2+}) = 0.28–0.36$ and Si in formula values = 6.15–6.57, and mainly fall inside the ferro-tschermarkite field (Fig. 5a; Leake et al., 1997). The amphiboles show a progressive decrease of Ca_{B} with increasing SiO_2 (Fig. 5b), consistent with the trend of typical magmatic or primary amphiboles (Mitchell, 1990; Pe-Piper, 2007).

4.3. Whole-rock geochemical and isotopic compositions

Major and trace element compositions of the ZTM Fe-rich mafic sills were listed in Table 3. The mafic sills have relatively high SiO_2 (50.11–53.19 wt.%), $\text{Fe}_{2}\text{O}_3^{\text{T}}$ (13.66–18.65 wt.%),

Table 2

Representative amphibole compositions of the ZTM Fe-rich mafic sills.

Sample	Amp-1	Amp-2	Amp-3	Amp-4	Amp-5	Amp-6	Amp-7	Amp-8	Amp-9	Amp-10	Amp-11	Amp-12	Amp-13	Amp-14
SiO ₂	40.25	40.63	41.04	40.43	40.83	40.18	44.20	40.37	43.38	42.29	39.99	41.85	41.36	40.15
TiO ₂	0.78	0.49	0.55	0.54	0.27	0.49	0.37	0.59	0.51	0.31	0.44	0.41	0.50	0.49
Al ₂ O ₃	12.76	13.03	12.64	12.88	13.23	13.09	9.37	13.06	11.06	12.16	13.11	11.60	12.02	13.14
FeO(T)	24.31	23.93	24.24	24.19	23.38	23.96	24.03	24.30	24.81	23.64	23.93	23.60	23.77	24.37
MnO	0.25	0.38	0.31	0.35	0.36	0.24	0.41	0.34	0.40	0.35	0.34	0.27	0.30	0.29
MgO	5.29	5.56	5.84	5.40	5.47	5.38	7.72	5.42	6.71	6.26	5.28	6.49	5.87	5.41
CaO	10.60	10.49	10.70	10.55	10.68	10.81	9.89	10.71	10.40	10.65	10.80	10.60	10.55	10.82
Na ₂ O	1.62	1.71	1.83	1.68	1.34	1.41	1.26	1.95	1.45	1.42	1.39	1.39	1.73	1.80
K ₂ O	0.66	0.68	0.58	0.73	0.61	0.74	0.37	0.68	0.49	0.52	0.66	0.52	0.57	0.70
Total	96.53	96.91	97.77	96.76	96.17	96.29	97.62	97.44	99.22	97.57	95.93	96.81	96.69	97.18
Si(T)	6.21	6.22	6.23	6.21	6.27	6.20	6.57	6.18	6.42	6.38	6.19	6.36	6.34	6.16
Al(iv)(T)	1.79	1.78	1.77	1.79	1.73	1.80	1.43	1.82	1.58	1.62	1.81	1.64	1.66	1.84
Al(vi)(T)	0.52	0.56	0.49	0.55	0.67	0.58	0.21	0.54	0.34	0.54	0.59	0.44	0.51	0.54
Fe ³⁺ (C)	0.95	1.00	0.99	0.98	0.95	0.94	1.50	0.90	1.28	1.04	0.97	1.11	0.92	0.93
Ti(C)	0.09	0.06	0.06	0.03	0.06	0.04	0.07	0.07	0.06	0.03	0.05	0.05	0.06	0.06
Mg-C	1.22	1.27	1.32	1.24	1.25	1.24	1.71	1.24	1.48	1.41	1.22	1.47	1.34	1.24
Fe2-C	2.18	2.06	2.08	2.13	2.05	2.15	1.48	2.21	1.78	1.94	2.13	1.89	2.13	2.20
Mn2-C	0.03	0.05	0.04	0.05	0.05	0.03	0.05	0.04	0.05	0.04	0.04	0.04	0.04	0.04
Ca-B	1.75	1.72	1.74	1.74	1.76	1.79	1.58	1.76	1.65	1.72	1.79	1.73	1.73	1.78
Na-B	0.25	0.28	0.26	0.26	0.24	0.21	0.36	0.24	0.35	0.28	0.21	0.27	0.27	0.22
Na-A	0.23	0.23	0.28	0.24	0.16	0.21	0.00	0.33	0.06	0.13	0.21	0.14	0.25	0.32
K-A	0.13	0.13	0.11	0.14	0.12	0.15	0.07	0.13	0.09	0.10	0.13	0.10	0.11	0.14
Sample	Amp-15	Amp-16	Amp-17	Amp-18	Amp-19	Amp-20	Amp-21	Amp-22	Amp-23	Amp-24	Amp-25	Amp-26	Amp-27	Amp-28
SiO ₂	40.28	41.29	42.15	45.71	42.45	40.20	41.55	38.33	41.34	42.07	42.92	42.73	40.55	43.06
TiO ₂	0.60	0.40	0.37	0.21	0.52	0.53	0.48	0.45	0.47	0.35	0.47	0.44	0.51	0.36
Al ₂ O ₃	13.21	12.17	12.33	8.23	13.46	13.43	12.28	11.56	12.41	11.85	11.24	11.39	12.87	11.33
FeO(T)	24.16	23.88	23.54	22.44	23.60	24.48	24.17	23.44	24.42	23.68	23.67	23.80	24.26	23.57
MnO	0.34	0.38	0.33	0.34	0.29	0.31	0.32	0.26	0.31	0.31	0.35	0.35	0.35	0.30
MgO	5.49	6.18	6.22	8.45	5.84	5.23	5.77	5.26	5.86	6.33	6.63	6.60	5.43	6.77
CaO	10.59	10.49	10.49	10.45	10.62	10.68	10.39	10.07	10.70	10.59	10.57	10.44	10.51	10.47
Na ₂ O	1.66	1.84	1.58	1.14	2.11	1.74	1.61	1.35	1.61	1.89	1.56	1.75	1.74	1.69
K ₂ O	0.69	0.55	0.53	0.27	0.66	0.87	0.54	0.68	0.60	0.52	0.51	0.47	0.62	0.48
Total	97.02	97.20	97.53	97.27	99.56	97.51	97.10	91.50	97.72	97.58	97.94	97.98	96.88	98.03
Si(T)	6.16	6.28	6.36	6.81	6.31	6.15	6.32	6.23	6.27	6.37	6.45	6.42	6.22	6.45
Al(iv)(T)	1.84	1.72	1.64	1.19	1.69	1.85	1.68	1.77	1.73	1.63	1.55	1.58	1.78	1.55
Al(vi)(T)	0.54	0.46	0.55	0.26	0.67	0.57	0.52	0.44	0.49	0.49	0.44	0.44	0.54	0.45
Fe ³⁺ (C)	1.04	1.07	1.03	1.13	0.76	0.95	1.06	1.11	1.04	0.94	1.02	1.06	1.01	1.04
Ti(C)	0.07	0.05	0.04	0.02	0.06	0.06	0.06	0.05	0.05	0.04	0.05	0.05	0.06	0.04
Mg-C	1.25	1.40	1.40	1.88	1.30	1.19	1.31	1.27	1.32	1.43	1.48	1.48	1.24	1.51
Fe2-C	2.06	1.97	1.94	1.66	2.17	2.18	2.02	2.07	2.05	2.06	1.95	1.93	2.10	1.91
Mn2-C	0.04	0.05	0.04	0.04	0.04	0.04	0.04	0.04	0.04	0.04	0.05	0.04	0.05	0.04
Ca-B	1.74	1.71	1.69	1.67	1.69	1.75	1.69	1.75	1.74	1.72	1.70	1.68	1.73	1.68
Na-B	0.26	0.29	0.31	0.33	0.31	0.25	0.31	0.25	0.26	0.28	0.30	0.32	0.27	0.32
Na-A	0.23	0.25	0.16	0.00	0.30	0.27	0.17	0.18	0.21	0.27	0.16	0.19	0.24	0.17
K-A	0.13	0.11	0.10	0.05	0.13	0.17	0.11	0.14	0.12	0.10	0.10	0.09	0.12	0.09

The amphibole's cations were calculated based on 23 oxygen atoms use the AMPH-CLASS (Esawi, 2004).

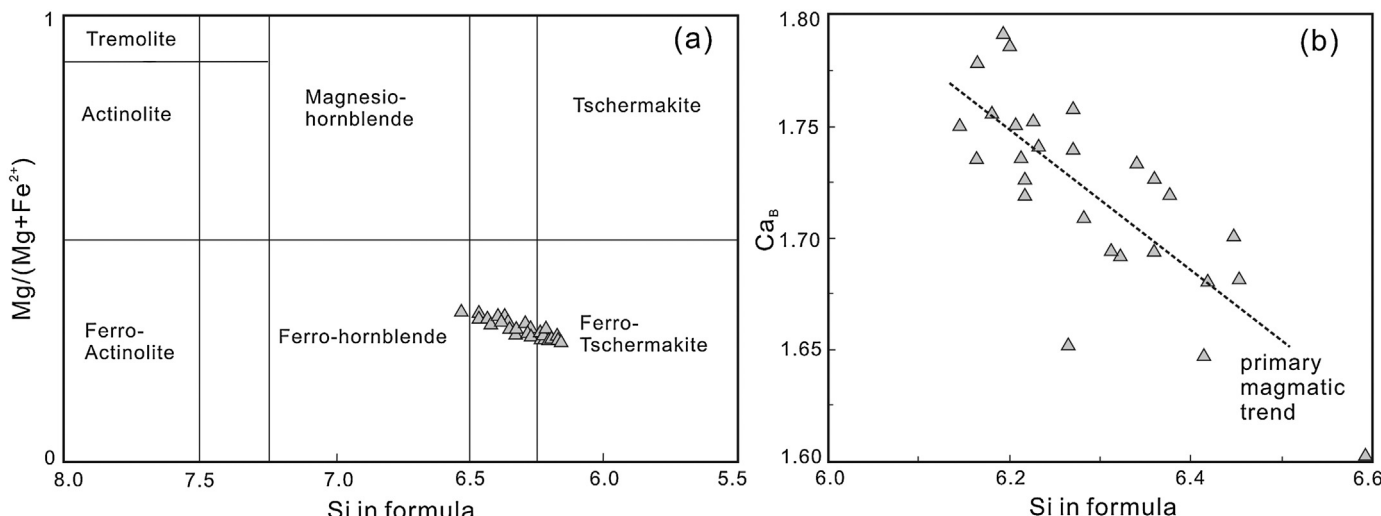
**Fig. 5.** (a) International Mineralogical Association (IMA) nomenclature (Leake et al., 1997) of the analyzed amphiboles; (b) plot of Ca_B vs. Si in formula, showing the primary/magmatic trend (Mitchell, 1990; Pe-Piper, 2007).

Table 3

Major and trace elemental compositions of the ZTM Fe-rich mafic sills.

Sample	HJ-1	HJ-2	HJ-3	HJ-4	HJ-5	HJ-6	HJ-7	HJ-8	HJ-9	HJ-10	HJ-11	HJ-12	HJ-13
SiO ₂	52.7	53.0	50.1	52.8	53.4	51.8	52.9	51.3	53.2	51.9	52.0	51.6	52.4
Al ₂ O ₃	12.4	11.8	13.6	12.0	12.4	11.7	13.8	12.8	12.1	13.4	14.0	14.0	13.0
Fe ₂ O _{3T}	16.9	18.1	15.8	18.0	17.1	18.7	13.7	16.1	16.7	15.3	14.2	14.4	17.5
CaO	7.20	6.97	7.45	7.00	6.66	7.04	8.10	7.52	6.84	7.53	7.19	7.61	6.27
MgO	4.32	3.53	4.94	3.45	3.77	3.64	4.39	4.43	4.22	4.58	4.62	4.75	4.10
Na ₂ O	3.31	3.08	3.06	3.04	3.64	2.64	3.89	3.18	3.04	3.06	3.80	3.45	3.37
K ₂ O	0.48	0.43	1.44	0.54	0.44	0.44	0.94	1.07	0.90	1.21	1.26	1.30	1.26
TiO ₂	1.74	1.96	1.43	2.12	1.60	2.97	1.25	1.43	1.54	1.48	1.35	1.28	1.55
MnO	0.31	0.32	0.30	0.31	0.30	0.29	0.24	0.26	0.28	0.25	0.23	0.25	0.28
P ₂ O ₅	0.19	0.22	0.16	0.21	0.16	0.21	0.13	0.14	0.16	0.15	0.12	0.13	0.16
LO.I	0.24	0.24	0.77	0.18	0.00	0.11	0.23	1.25	0.58	0.66	0.74	0.79	0.27
Total	99.8	99.7	99.1	99.7	99.5	99.5	99.5	99.5	99.5	99.5	99.5	99.5	100
Sc	39.1	34.2	33.2	35.0	44.7	49.8	35.7	38.3	40.3	39.7	40.3	40.6	43.8
Ti	8909	9933	7133	10,581	9178	17,159	8092	7190	8262	8510	7526	7392	9086
V	312	303	256	306	298	474	272	248	268	271	256	264	310
Cr	17.2	15.0	32.6	12.0	225	210	191	102	102	130	118	135	176
Mn	2183	2256	2073	2183	2298	2251	1918	1827	1980	1889	1722	1872	2124
Co	51.7	62.8	56.3	49.8	48.9	52.2	48.1	49.8	57.0	50.1	48.2	54.7	55.9
Ni	23.0	17.5	45.2	15.3	38.9	33.1	37.3	45.9	43.5	46.5	41.8	50.0	35.6
Cu	165	381	67	169	165	424	241	326	359	35.4	83.2	165	144
Zn	197	167	211	180	166	160	201	191	210	195	197	213	214
Ga	20.4	22.4	19.6	22.3	21.5	21.8	19.7	19.6	20.3	19.8	19.0	20.6	21.9
Ge	2.05	2.26	1.84	2.22	2.49	2.66	1.87	2.03	2.22	2.03	1.84	2.00	2.20
Rb	7.88	3.45	37.59	7.99	5.57	2.89	23.6	26.5	31.0	34.5	40.9	38.1	47.2
Sr	72.5	58.1	132.7	68.2	83.9	93.9	83.4	230	169	194	211	247	116
Y	34.9	40.1	29.0	40.2	39.9	42.8	32.4	35.0	37.2	35.7	33.3	33.6	40.6
Zr	163	179	130	199	152	187	156	132	124	139	111	117	140
Nb	7.19	8.01	5.71	9.07	6.37	9.13	6.02	4.96	5.50	5.71	5.22	4.92	6.05
Cs	0.43	0.18	1.92	0.48	0.30	0.08	1.56	1.44	1.80	1.62	2.36	1.68	3.19
Ba	101	84.9	556	84.2	68.2	145	220	298	335	457	438	551	395
La	18.0	26.1	14.9	20.5	16.6	20.6	14.0	13.3	14.5	15.1	11.7	12.9	16.0
Ce	40.3	58.1	32.8	45.9	36.6	45.0	31.4	30.1	33.0	34.1	26.6	29.3	36.4
Pr	5.48	7.89	4.56	6.37	4.96	6.15	4.13	3.89	4.30	4.43	3.43	3.80	4.78
Nd	24.1	33.6	19.9	27.4	21.2	26.4	17.5	16.9	18.5	19.1	15.3	16.4	20.7
Sm	5.50	7.52	4.70	6.46	5.11	6.24	4.58	4.16	4.59	4.48	3.74	4.09	4.98
Eu	1.66	2.20	1.39	1.90	1.62	1.84	1.53	1.39	1.52	1.47	1.23	1.37	1.64
Gd	6.72	8.32	5.45	7.44	5.60	6.90	5.60	4.81	5.43	5.18	4.49	4.72	5.81
Tb	1.10	1.39	0.95	1.31	0.98	1.16	0.98	0.86	0.95	0.90	0.82	0.84	1.03
Dy	6.98	8.12	5.81	7.73	6.04	6.74	6.00	5.19	5.86	5.56	5.12	5.12	6.34
Ho	1.49	1.73	1.25	1.70	1.30	1.36	1.29	1.11	1.25	1.18	1.09	1.09	1.34
Er	4.10	4.47	3.31	4.67	3.68	3.70	3.55	3.09	3.39	3.16	3.04	3.06	3.73
Tm	0.58	0.67	0.49	0.68	0.54	0.54	0.52	0.45	0.51	0.45	0.45	0.45	0.54
Yb	3.71	4.32	2.96	4.39	3.54	3.53	3.31	2.83	3.11	2.95	2.92	2.84	3.44
Lu	0.55	0.64	0.46	0.65	0.52	0.55	0.49	0.44	0.47	0.45	0.43	0.42	0.51
Hf	4.13	4.60	3.31	4.94	4.26	5.10	4.19	3.70	3.48	3.84	3.21	3.32	4.06
Ta	0.53	0.58	0.40	0.65	0.44	0.62	0.44	0.39	0.40	0.41	0.37	0.37	0.43
Pb	1.53	1.52	1.14	1.58	4.54	4.75	0.92	4.87	4.77	4.91	4.67	4.91	3.02
Th	3.55	4.11	2.78	4.31	3.44	4.10	3.53	2.92	2.70	3.05	2.43	2.59	3.22
U	0.81	0.99	0.76	0.99	0.81	1.08	0.76	0.71	0.78	0.80	0.64	0.67	0.82

TiO₂ (1.25–2.97 wt.%), CaO (6.71–8.1 wt.%) and low MgO (3.64–4.94 wt.%) contents. On the Nb/Y vs. SiO₂ diagram (Winchester and Floyd, 1977), data points fall into the sub-alkaline basalt field (Fig. 6a). Similarly, based on the classification of Jensen (1976), the sills were plotted inside the high-Fe tholeiitic basalt field (Fig. 6b). The ZTM Fe-rich mafic sills have Cr and Ni contents in the ranges of 12–225 ppm and 15–50 ppm, respectively (Table 3). Primitive-mantle normalized trace element spider diagrams show that all the samples have significant Nb and Ta depletions, and weakly negative Ti anomalies (Fig. 7a). Some samples show relatively low Rb, Ba and K, which may be caused by their low biotite content (Fig. 3b and c). All the samples display smoothly right dipping REE patterns with (La/Yb)_N = 2.88–4.32 and (La/Sm)_N = 1.97–3.46, without obvious Eu anomalies (Eu* = 0.83–0.95) (Fig. 7b).

Nd-Hf isotopic compositions for the ZTM Fe-rich mafic sills were listed in Table 4. The initial ¹⁴³Nd/¹⁴⁴Nd and ε_{ND}(t) (t = 1900 Ma) values range from 0.512192 to 0.5120302 and 0.3 to 2.4, respectively. The initial ¹⁷⁶Hf/¹⁷⁷Hf ratios range from 0.281747 to

0.281632 and the ε_{Hf(t)} (t = 1900 Ma) for these samples range from 2.1 to 6.1.

5. Discussion

5.1. Crustal contamination and crystal fractionation

Element mobility is a major concern in geochemical study of Precambrian igneous rocks. To minimize the late alteration influence, we have focused on the less mobile high field strength elements (HFSEs) and rare earth elements (REEs). In contrast, the more mobile large ion lithophile elements (LILEs) such as Cs, Rb, Sr and K were not discussed here (e.g., Muecke et al., 1979; Weaver and Tarney, 1981; Sheraton, 1984; Jochum et al., 1991).

Crustal contamination and fractional crystallization must be considered before evaluating the role of mantle sources for the ZTM Fe-rich mafic sills. Xu et al. (2003) proposed that contamination of crustal materials, especially these in the upper continental crust, may increase oxygen fugacity (fO₂) and thereby leads to

Table 4
Nd–Hf isotopic compositions of the ZTM Fe-rich mafic sills.

Sample	$^{147}\text{Sm}/^{144}\text{Nd}$	$^{143}\text{Nd}/^{144}\text{Nd}$	2σ	$(^{143}\text{Nd}/^{144}\text{Nd})_i$	$\varepsilon_{\text{Nd}}(t)$	$T_{\text{DM},2}(\text{Ma})$	$^{176}\text{Lu}/^{177}\text{Hf}$	$^{176}\text{Hf}/^{177}\text{Hf}$	2σ	$(^{176}\text{Hf}/^{177}\text{Hf})_i$	$\varepsilon_{\text{Hf}}(t)$	$T_{\text{DM}}(\text{Ma})$	ΔHf	
HJ-1	0.1380	0.512028	0.000003	0.510302	2.4	2177	/	/	/	/	/	/	/	/
HJ-2	0.1353	0.511925	0.000003	0.510233	1.1	2286	/	/	/	/	/	/	/	0.5
HJ-3	0.1427	0.512031	0.000003	0.510247	1.3	2264	0.0193	0.282414	0.000003	0.281717	5.1	2297	0.5	
HJ-4	0.1424	0.512023	0.000003	0.510243	1.3	2270	0.0183	0.282294	0.000003	0.281632	2.1	2494	-3.5	
HJ-5	0.1457	0.512014	0.000003	0.510192	0.3	2351	0.0169	0.282288	0.000003	0.281677	3.7	2349	-3.5	
HJ-6	0.1430	0.512019	0.000003	0.510231	1.0	2290	0.0150	0.282208	0.000003	0.281668	3.4	2331	-6.5	
HJ-8	0.1487	0.512080	0.000003	0.510220	0.8	2306	0.0164	0.282280	0.000003	0.281688	4.1	2312	-5.5	
HJ-9	0.1500	0.512085	0.000003	0.510210	0.6	2323	0.0188	0.282386	0.000003	0.281707	4.8	2313	-1.9	
HJ-10	0.1419	0.512040	0.000003	0.510265	1.7	2235	0.0175	0.282336	0.000004	0.281706	4.7	2290	-2.5	
HJ-13	0.1453	0.512077	0.000003	0.510261	1.6	2242	0.0174	0.282374	0.000004	0.281747	6.2	2188	-2.1	

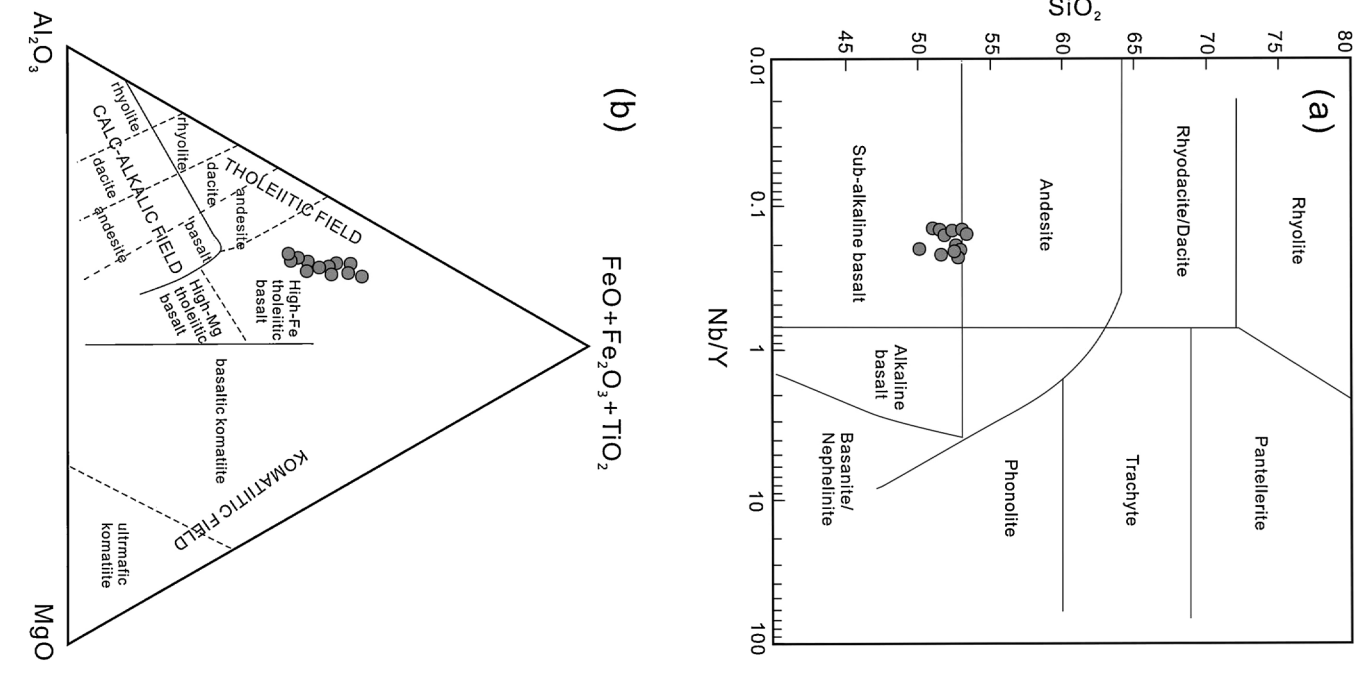


Fig. 6. (a) SiO_2 vs. Nb/Y diagram (after Winchester and Floyd, 1977); (b) $(\text{FeO} + \text{Fe}_2\text{O}_3 + \text{TiO}_2) - \text{Al}_2\text{O}_3 - \text{MgO}$ ternary plot (after Jensen, 1976) of the ZTM Fe-rich mafic sills.

early magnetite crystallization, which consequently lowers the Fe content of the magma. In the case of the ZTM Fe-rich mafic sills, negative MgO and $\text{Fe}_{2\text{O}}^{\text{T}}$ correlation (Fig. 8c) and the absence of xenocrystic zircon argue against significant crustal contamination (e.g., Wang et al., 2004, 2008; Zhang et al., 2013b). Furthermore, the ZTM Fe-rich mafic sills have higher $\text{Fe}_{2\text{O}}^{\text{T}}$ ($>13.66\text{ wt}\%$) and TiO_2 ($>1.25\text{ wt}\%$) but lower Al_2O_3 ($<14\text{ wt}\%$) than the average continental crust ($\text{FeO}^{\text{T}} = 6.71\text{ wt}\%$, $\text{TiO}_2 = 0.72\text{ wt}\%$, $\text{Al}_2\text{O}_3 = 15.9\text{ wt}\%$; Rudnick and Gao, 2003). Therefore, significant crustal assimilation was unlikely.

The ZTM Fe-rich mafic sills represent fractionated melts, as indicated by their low MgO ($<5.0\text{ wt}\%$), Ni ($15\text{--}50\text{ ppm}$) and Cr ($12\text{--}25\text{ ppm}$) (Table 3). These characteristics suggest that these

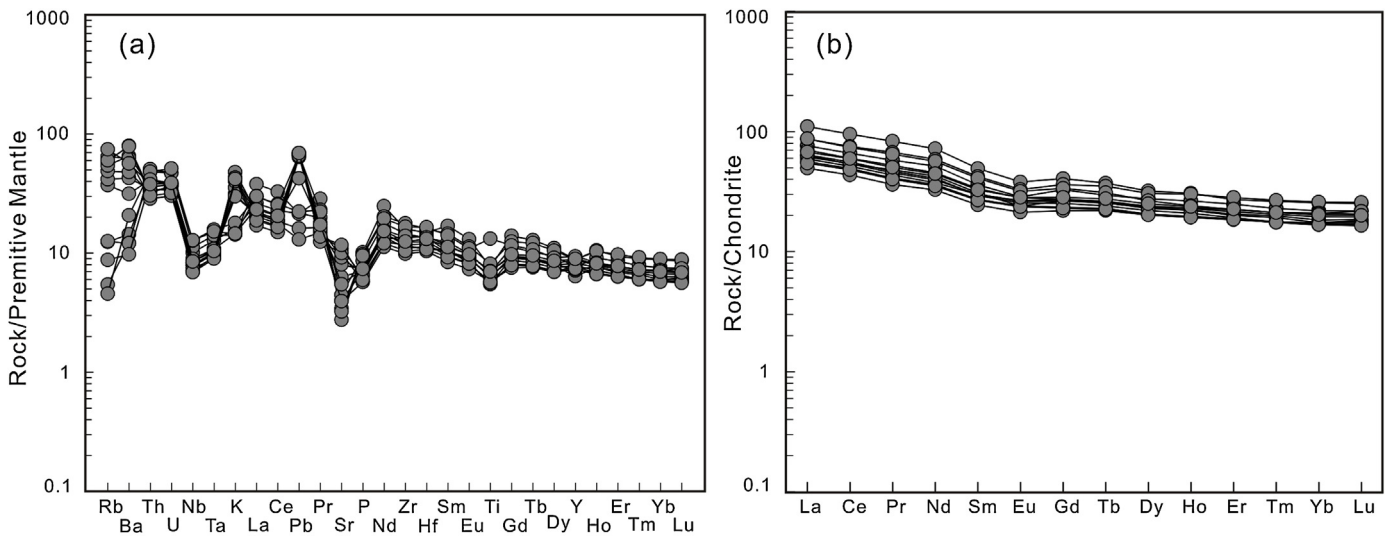


Fig. 7. (a) Rock/primitive mantle diagram for ZTM Fe-rich mafic sills; (b) REE/Chondrite diagram for the ZTM Fe-rich mafic sills. Chondrite and primary mantle values from Sun and McDonough (1989).

sills have experienced certain degrees of fractional crystallization during their ascent. MgO correlates positively with Al₂O₃, CaO and Ni, indicating that olivine and/or clinopyroxene crystallization may have occurred (Fig. 8b, e and i). Negative MgO vs. CaO/Al₂O₃ correlation indicates that clinopyroxene was not a major

crystallizing phase (e.g., Mayer et al., 2013; Zhang et al., 2013b). The insignificant Eu anomalies ($\text{Eu}^* = 0.83\text{--}0.95$, Fig. 7b) may reflect the very minor plagioclase segregation/accumulation. Negative correlations between MgO and TiO₂, and between MgO and Fe₂O₃^T (Fig. 8 c and f) illustrate that the fractionation of Fe-Ti oxides was

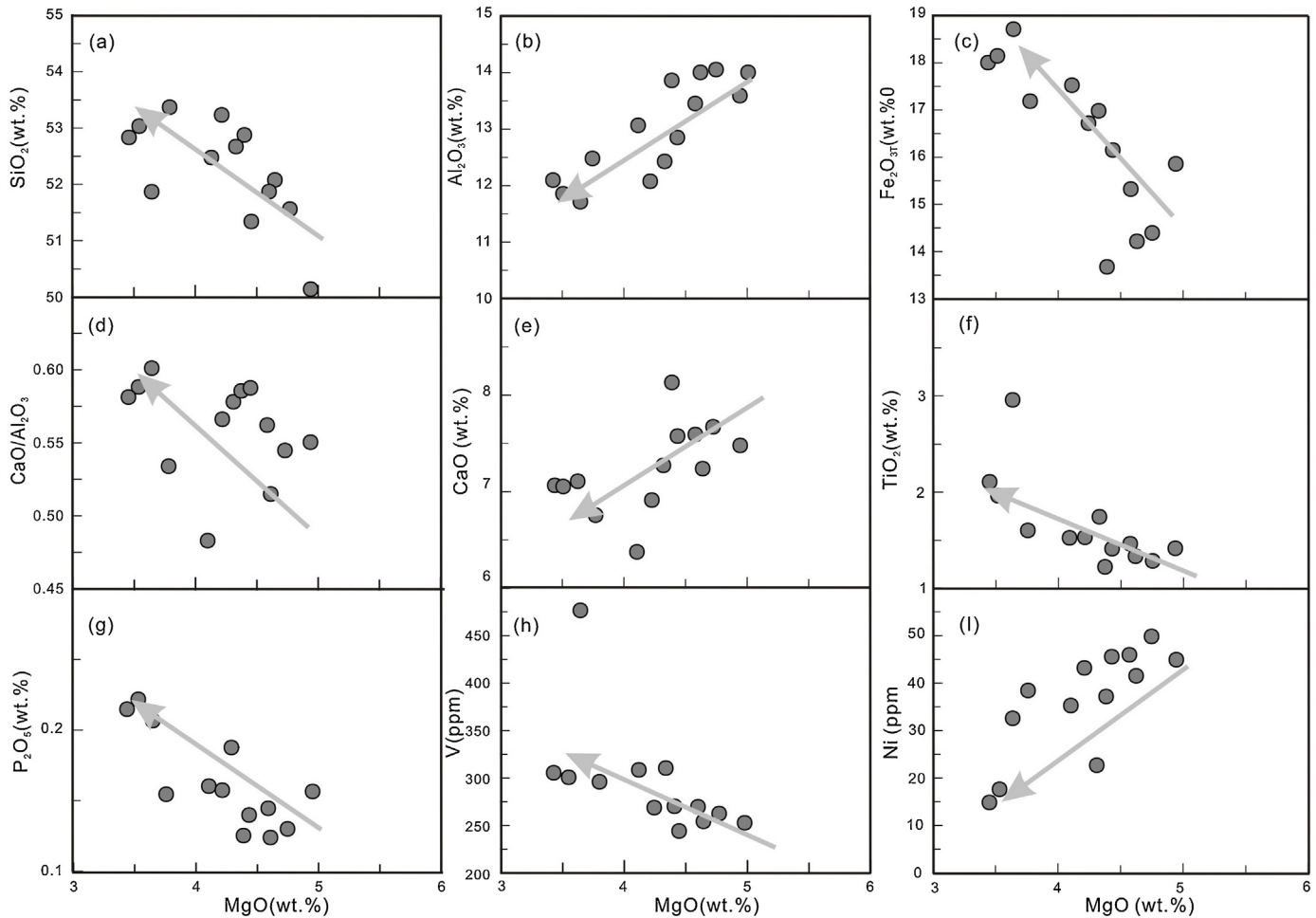


Fig. 8. Major and trace element plots against MgO (as fractionation index) diagrams for the ZTM Fe-rich mafic sills.

insignificant (e.g., Wang et al., 2008). The distinctive increase of vanadium (V) with decreasing MgO (Fig. 8h) further indicates the insignificant Fe–Ti oxides fractional crystallization, because V in the magma is largely controlled by the fractionation/accumulation of Fe–Ti oxides (Jang et al., 2001). Similarly, P₂O₅ also increases with decreasing MgO (Fig. 8g), indicating that the fractionation of apatite was not significant either (Wang et al., 2008). Therefore, the P and Ti depletions in the mafic sills were probably inherited from their parental magma rather than the result of apatite and Fe–Ti oxides fractionation. Consequently, we suggest that many of the variations in major and trace element contents cannot be explained by fractional crystallization alone.

5.2. Source nature of the ZTM Fe-rich mafic sills

Based on the discussion above, we conclude that the generation of the weakly altered ZTM Fe-rich mafic sills has been influenced by moderate olivine fractional crystallization and insignificant crustal assimilation. To minimize the fractional crystallization influence, we have used the HFSE and REE abundance and ratios (e.g., La/Sm, La/Yb) to determine the nature of the sills' magma source (e.g., Wang et al., 2003, 2004, 2008; Zhu et al., 2010; Erkul and Erkul, 2012; Peng et al., 2013; Zhang et al., 2013b).

The ZTM Fe-rich mafic sills are LREE-enriched and HFSE depleted, showing low (Nb/La)_N and (Nb/Zr)_N values (Fig. 7 and Table 3). In the $\varepsilon_{\text{Hf}}(t)$ vs. $\varepsilon_{\text{Nd}}(t)$ diagram, the sills are plotted in the overlap field of Ocean Island Basalt (OIB) and global lower crust (Fig. 9). The ZTM Fe-rich mafic sills also have stable and old Hf and Nd model age, indicating the involvement of older crustal materials in the source (e.g., Wang et al., 2008; Zhang et al., 2012b). These characteristics suggest that the sills have an enriched mantle source. The lithospheric mantle beneath Proterozoic terranes has been broadly refertilized by metasomatic processes (Tang et al., 2011 and references therein). In general, depletion of Ta relative to La has been suggested to be resulted from mantle metasomatism by subduction-related processes (La Flèche et al., 1998; Wang et al., 2004), through the circulation of carbonatic- or subduction-melts/fluids (Elliott et al., 1997; Plank and Langmuir, 1998; Class et al., 2000; Kogarko et al., 2001; Reubi et al., 2014). Magmas derived from a carbonate-metasomatized mantle are usually characterized by being ultramafic and having low (Hf/Sm)_N values (La Flèche et al., 1998; Kogarko et al., 2001; Gasparik and Litvin, 2002; Hammouda, 2003), which are inconsistent with the ZTM Fe-rich mafic sills and thus their mantle source was unlikely to have been

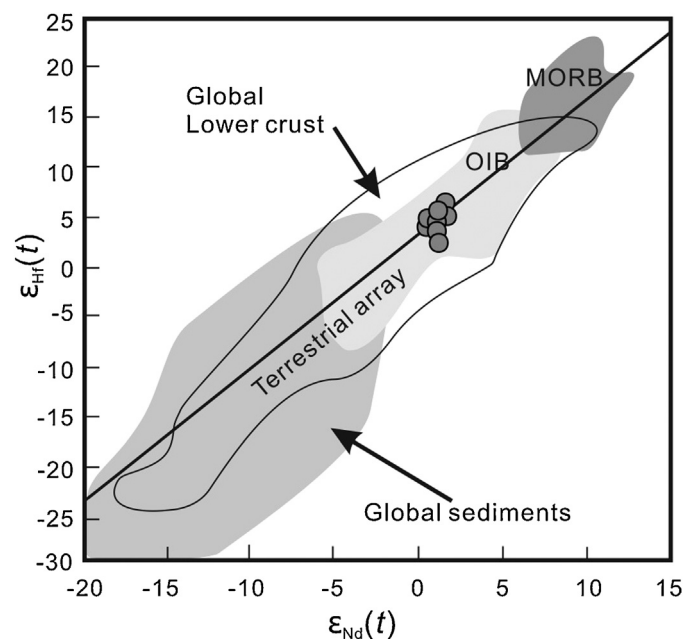


Fig. 9. Plots of $\varepsilon_{\text{Hf}}(t)$ vs. $\varepsilon_{\text{Nd}}(t)$ for the ZTM Fe-rich mafic sills (after Dobosi et al., 2003). “Terrestrial array” as defined by Vervoort et al. (1999) (MORB: mid-ocean ridge basalt; OIB: ocean island basalt).

metasomatized by carbonatic fluids (Fig. 10a). In the Th/La vs. Ce/Pb diagram (Fig. 10b), the data points fall along a trend consistent with what would be expected for fluid-related metasomatism (e.g., Temizel et al., 2012).

The highly incompatible La and the less incompatible Sm contents were used to constrain the bulk composition of the source, as La and Sm are not significantly controlled by the source mineralogical variations (Aldanmaz et al., 2000; Green, 2006; Zhu et al., 2009; Yang et al., 2012). The ZTM Fe-rich mafic sills have La abundances and La/Sm values greater than those generated by depleted- or primitive mantle melting (Fig. 11a). The partial melting trajectory for the ZTM Fe-rich mafic sills implies a ~10% partial melting of an enriched mantle that contains mainly spinel lherzolite (e.g., Green, 2006; Zhu et al., 2009; Yang et al., 2012). Sm/Yb values are sensitive to the source mineralogy, because Yb is compatible with garnet but not with either clinopyroxene or spinel. The Yb concentration and Sm/Yb values of the ZTM Fe-rich mafic sills are plotted along

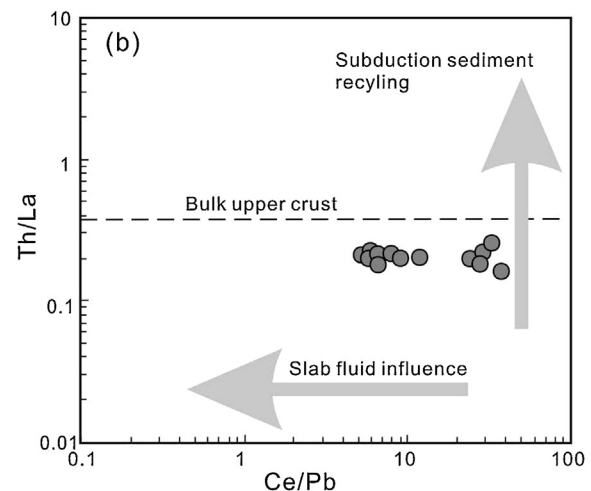
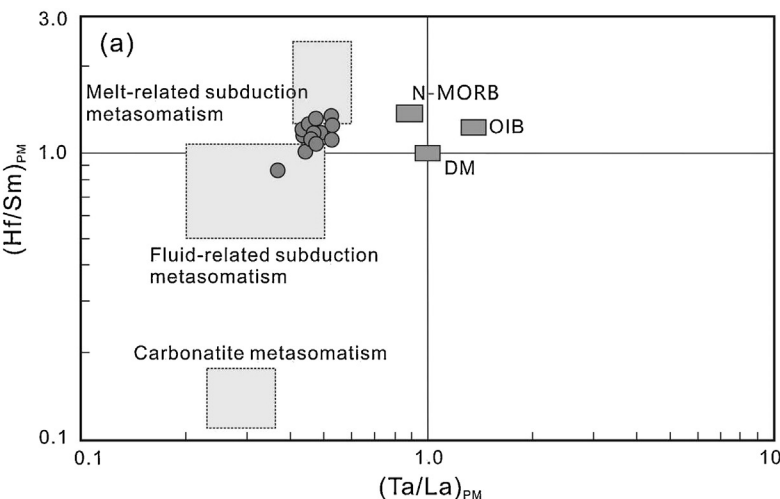


Fig. 10. Co-variation diagrams of (a) $(\text{Hf/Sm})_{\text{PM}}$ vs. $(\text{Ta/La})_{\text{PM}}$ (after La Flèche et al., 1998); and (b) Th/La vs. Ce/Pb ((Temizel et al., 2012), illustrating that the source region of the ZTM Fe-rich mafic sills has been influenced by subduction-related fluids.

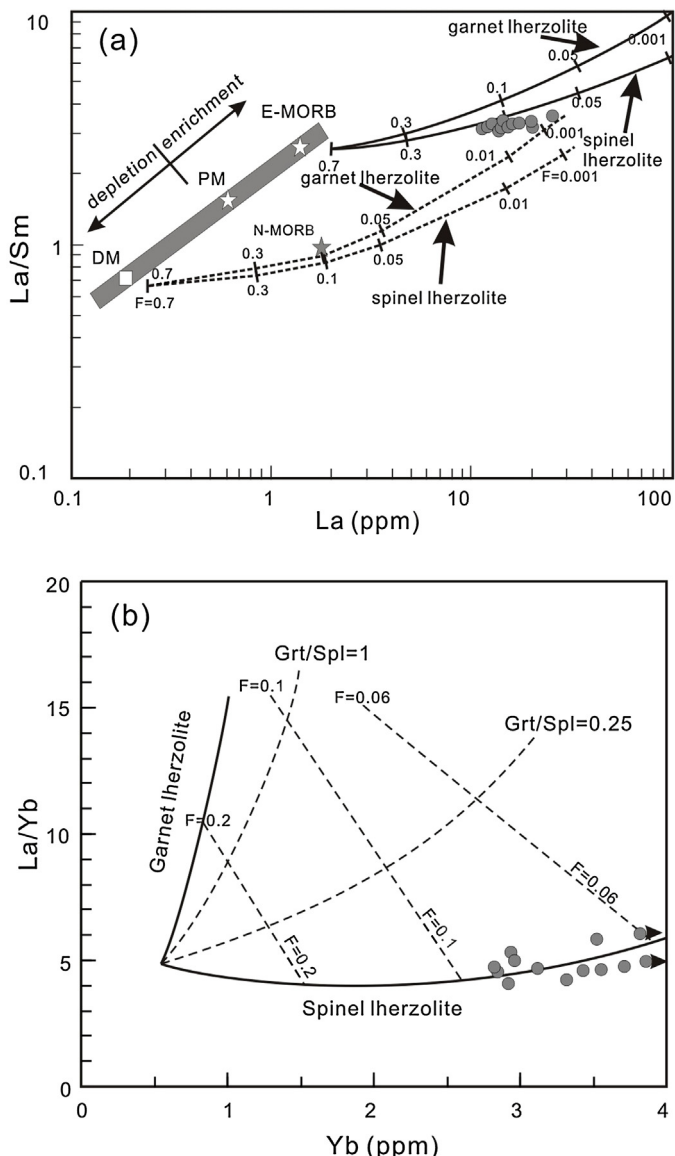


Fig. 11. Plot of (a) La/Sm vs. La and (b) La/Yb vs. Yb for the ZTM Fe-rich mafic sills (for details, see Zhu et al., 2009).

the curve of partial melting of spinel lherzolite (Fig. 11b), which further supports a spinel lherzolite source. As a conclusion, the mantle source of the Fe-rich mafic sills was likely to be a lithospheric one, metasomatized by subduction-related fluids and mainly composed of spinel lherzolite.

5.3. Formation mechanism of the ZTM Fe-rich mafic sills

The petrogenesis of Fe-rich rocks is still enigmatic, with several models being proposed to explain their high-Fe contents: (1) Low degree partial melting of the mantle at high-pressure (Hirose and Kushiro, 1993; Lassiter and DePaolo, 1997); (2) High degree partial melting of a refractory subducted slab at low pressure (Leybourne et al., 1999); (3) High degree partial melting of a peridotite–basalt mixture (Kogiso et al., 1998; Wang et al., 2008); (4) Inheritance from a high-Fe mantle source, e.g., involvement of subducted Fe–Mn nodules (Baker and Krogh Jensen, 2004) or a mantle plume related Fe-rich streaks (Kerrich et al., 1999; Gibson et al., 2000; Gibson, 2002).

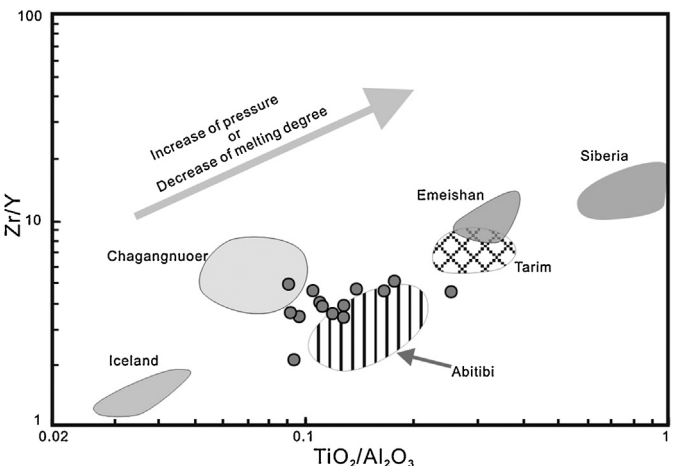


Fig. 12. Plot of Zr/Y vs. TiO₂/Al₂O₃ (Ichiyama and Ishiwatari, 2005; Ichiyama et al., 2006) for the ZTM Fe-rich mafic sills. Picrites from Iceland in middle (Skovgaard et al., 2001), Fe-rich basalts form Abitibi (Kerrich et al., 2008), Chagangnuoer (Another's unpublished data), Tarim (Jiang et al., 2004), Emeishan (Xu et al., 2003) and Siberian (Arndt et al., 1995) are shown for comparison.

The Zr/Y vs. Al₂O₃/TiO₂ co-variation diagram (Ichiyama and Ishiwatari, 2005) has been used to estimate the pressure of partial melting. In the diagram, picrites generated at spreading ridges in Iceland (Skovgaard et al., 2001), Fe-rich basalt generated in back-arc basin settings from Changangnuoer (Another's unpublished data) and Abitibi (Kerrich et al., 2008) and Fe-rich basalts generated in continental settings in Tarim (Jiang et al., 2004) and Emeishan (Xu et al., 2003) and picrites in Siberian (Arndt et al., 1995) were plotted along a trend of increasing pressure (Fig. 12). Partial melting pressure of the ZTM Fe-rich mafic sills resembles that of the Abitibi and Chagangnuoer Fe-rich basalts (Fig. 12), suggesting that the sills may have formed at a relatively low pressure. Leybourne et al. (1999) suggested that Fe-rich magmas derived from a refractory subducted slab source would have positive Nb, Ta and Ti anomalies due to the slab having been extracted by previous arc-related magmatism, however, positive Nb, Ta and Ti anomalies is absent in the ZTM Fe-rich mafic sills (Fig. 7a). Partial melting of a peridotite–basalt mixture may generate Fe-rich magmas (Kogiso et al., 1998). Sobolev et al. (2007) have estimated the amount of recycled crust in the sources of mantle-derived melts and suggested the involvement of 2–20% (and up to 28%) of recycled crust. However, ~10% partial melting of such a peridotite–basalt mixture (with ~30% basalt) produces a melt with FeO^T content no more than 12 wt.% (Kogiso et al., 1998). Subduction of Fe–Mn nodules and their subsequent injection into the mantle is another possible way for the Fe-enrichment in sub-continental mantle (Baker and Krogh Jensen, 2004). Nevertheless, if such process has occurred, the magma of the ZTM Fe-rich mafic sills would also be Mn-enriched (Ichiyama et al., 2006), which is inconsistent with our new geochemical data. In addition, Fe–Mn nodules have commonly decoupled Nd–Hf isotope values (Vervoort et al., 1999; Chauvel et al., 2009). If Fe–Mn nodules have entered into the mantle source, the Nd and Hf isotopes would be deviated from the terrestrial array, which is again not supported by our new data (Fig. 9). Another possible source for Fe-rich mafic rocks is the Fe-rich streaks related to mantle plumes (Kerrich et al., 1999; Gibson et al., 2000; Gibson, 2002). However, Fe-rich magmas derived from Fe-rich streaks have commonly high ε_{Nd}(t) (up to +6) and (Nb/La)_{PM} (>1, Gibson, 2002 and references therein), contrasting with our new isotopic data, i.e., low ε_{Nd}(t) (< 3) and (Nb/La)_{PM} (<0.5). It is thus clear that the ZTM Fe-rich mafic sills were unlikely to have been produced by partial melting of Fe-rich streaks.

An alternative way to generate Fe-rich magmas is that the magmas have evolved under low oxygen fugacities (f_{O₂}), which would

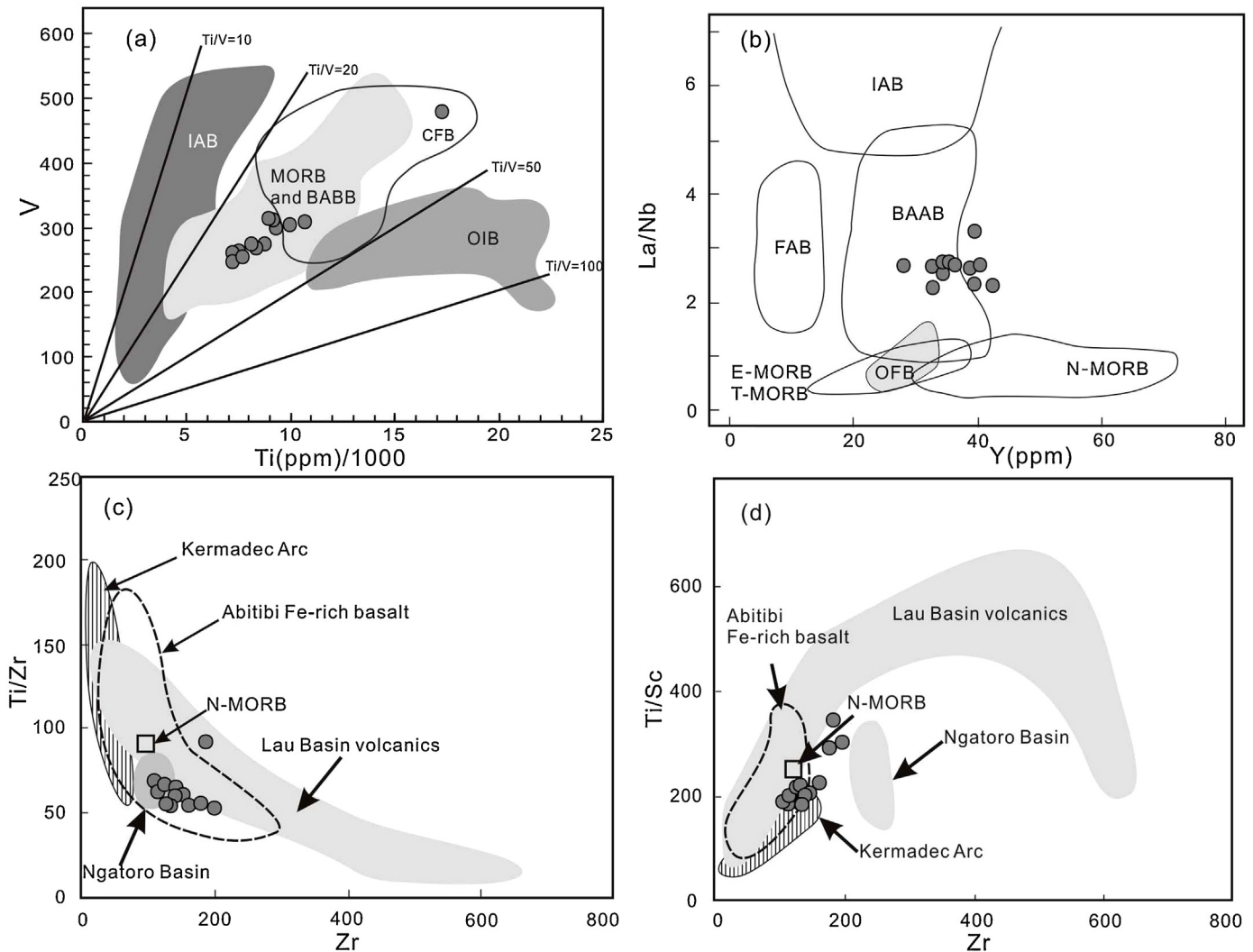


Fig. 13. Tectonic discrimination diagrams for the ZTM Fe-rich mafic sills. (a) V vs. $Ti/1000$ diagram (Shervais, 1982); (b) La/Nb vs. Y diagram (Floyd et al., 1991); (c) Ti/Zr vs. Zr diagram (Kerrick et al., 2008); and (d) Ti/Sc vs. Zr diagram (Kerrick et al., 2008). Date for the Lau Basin- and Abitibi volcanics from Pearce et al. (1994) and Kerrich et al. (2008), respectively. The fields for Kermadec and Ngatoro from Gamble et al. (1994) (BABB: back-arc basin basalts; E-MORB: enriched MORB; T-MORB: transitional MORB; N-MORB: normal MORB; CFB: continental flood basalts; FAB: fore-arc platform basalts; IAB: island arc basalts; OFB: oceanic flood basalts; OIB: ocean island basalts).

delay the Fe-Ti oxide crystallization and promotes Fe-Ti enrichment in the residual magmas (e.g., Xu et al., 2003; Rutherford et al., 2006; Peng et al., 2007, 2013). In the Fig. 8, the Fe and Ti increase distinctly with decreasing MgO, suggesting that the magmas may have evolved in a low fO_2 environment (e.g., Peng et al., 2013). As discussed above, the mantle source of the ZTM Fe-rich mafic sills has been metasomatized by subduction-related fluids, which are widely considered to play a critical role in subduction zones and significantly influence the fO_2 of the mantle wedges (e.g., Peacock, 1990; You et al., 1996; Kelley and Cottrell, 2009; Rowe et al., 2009). Uranium (U) behaves generally similar to the LILEs. It is proposed that enrichment of U over Th is present in subduction-related fluids (Ayers, 1998; Jiang et al., 2009), hence magmas derived from a metasomatized mantle wedge may show relative low Th/U (Bali et al., 2011). However, the ZTM Fe-rich mafic sills have higher Th/U than those of the average MORB (~3.0), OIB (~3.4) and IAB (~2, Hawkesworth et al., 1991) but lower than average crustal rocks (~5.0, Rudnick and Fountain, 1995). As significant crustal contamination has been ruled out in the previous discussion, another possible way to interpret the high Th/U of the ZTM Fe-rich mafic sills is that the subduction-related fluids may have low fO_2 . fO_2 is a critical controlling factor for Th/U fractionation in subduction-related fluids (Bali et al., 2011). In low fO_2 fluids, since both U and Th are

poorly soluble in water in the +4 oxidation state, the fractionation of Th/U would be insignificant. If the fluids have high fO_2 , U may be oxidized to U^{6+} and readily soluble in fluids as uranyl (UO^{2+}) cation (Bali et al., 2011). This provided further evidence that the magma may have a low fO_2 environment. The widely distributed black schist in the ZTM (Sun and Hu, 1993; Bai et al., 1997) may be account for the occurrence of low fO_2 subduction-related fluids. Subduction-related fluids could transport Fe as dissolved species (Philippot and Selverstone, 1991) and leach Fe from the subducted slab and the lower part of the mantle wedge into the upper part of mantle wedge during their ascent (e.g., Li et al., 2013a; Ling et al., 2013), which would increase the Fe and H_2O contents in the upper part of the mantle wedge. To conclude, we suggest that the ZTM Fe-rich mafic sills were originated from the partial melting of a Fe-rich mantle wedge, which generated a relatively high Fe parental magma. This parental magma may have then evolved under a low fO_2 , resulting in further Fe-enrichment and eventually produced the Fe-rich mafic sills.

5.4. Tectonic settings and geodynamic implications

Fe-rich magmas have higher density than typical subduction-related magma, thus their transport to the earth's surface requires

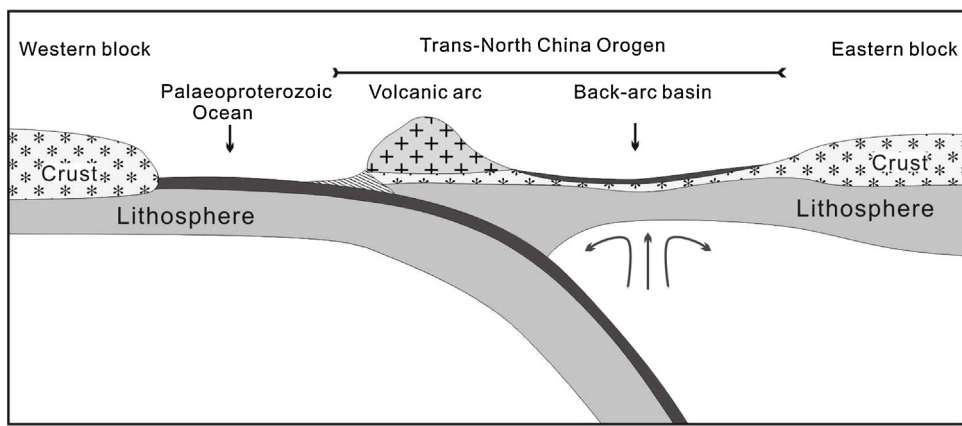


Fig. 14. Simplified cartoon showing the development of the Paleoproterozoic back-arc basin in the Trans-North China Craton.

extensional environments (Brooks et al., 1991), such as mid-oceanic ridges (Leroex et al., 1982; Brooks et al., 1991), continental rifts (Gibson et al., 2000; Skovgaard et al., 2001; Xu et al., 2003; Jiang et al., 2004; Peng et al., 2007), back-arc basins (Leybourne et al., 1999; Kerrich et al., 2008) and post-collisional extension settings (Wang et al., 2004, 2008). Depletions in Nb-Ta and Ti are typical of subduction-related magmatism. Since no ZTM Fe-rich mafic sills were found intruding into the ~2500 Ma Sushui TTG gneisses (Fig. 1b), implying that the sills were unlikely to have formed in a within plate setting. In addition, the amphiboles in the Fe-rich mafic sills have relatively low TiO_2 and Na_2O contents, suggesting that they were formed in subduction-related settings (Coltorti et al., 2007).

Most ZTM Fe-rich mafic sills have flat REE patterns (Fig. 7b) and positive $\varepsilon_{Nd}(t)$ values, suggesting that the sills may have been generated in a subduction-related extensional regime, such as back-arc basins (e.g., Gribble et al., 1996; Keller et al., 2002; Ilnicki et al., 2013). Ti/V values (28–36) of the ZTM Fe-rich mafic sills fell into an overlapped area of MORB and BABB (Fig. 13a). In the La/Nb vs. Y tectonic discrimination diagram (Fig. 13b), most Fe-rich mafic sills samples were plotted in the BABB area. These characteristics imply that the ZTM Fe-rich mafic sills were generated in a back-arc basin setting. Based on the geochemical data from modern paired arcs to back-arc basin setting, Woodhead et al. (1993) and Gamble et al. (1994) proposed that the Ti/Zr vs. Zr and Ti/Sc vs. Zr discrimination diagrams (Fig. 13c and d) can effectively distinguish the basalts originated from arcs from those originated in their associated back-arc basins. The back-arc basalt data are generally plotted between the MORB and OIB fields, and tend to be less hydrous with subdued HFSE/REE fractionations (Kerrich et al., 2008). With these diagrams, Kerrich et al. (2008) suggested that the Fe-rich basalts from the Abitibi greenstone belts in Canada were produced in back-arc environment. Data of the ZTM Fe-rich mafic sills are plotted in the field of the Abitibi Fe-rich basalts in both discrimination diagrams (Fig. 13c and d), indicating that they were also produced in a back-arc basin setting. Regionally, nearly contemporaneous (~1841 Ma) back-arc basin rocks has been reported in western Shandong (Wang et al., 2007), suggesting that before the final collision between the Western- and Eastern blocks, an extensional tectonic regime may have occurred in the central NCC (Kröner et al., 2006). The contemporaneous sedimentary strata in the ZTM are the Zhongtiao Group. The Lower Zhongtiao Subgroup was deposited in a back-arc basin whereas the Upper Zhongtiao Subgroup was deposited in a foreland basin (Li et al., 2011; Liu et al., 2012, 2014). Therefore, we can conclude an arc-back-arc basin system may have existed in the ZTM. Although coeval arc-related rocks in the ZTM have not yet been identified, we cannot preclude their existence since extensive and detailed regional geochemical survey is not yet available.

In the previous studies, coeval mafic dikes in Huai'an and Lvliang have been suggested to have formed in arc-related settings (Peng et al., 2005; Kröner et al., 2006; Zhao et al., 2008; Wang et al., 2014), or more precisely in an extensional setting before the final amalgamation of the Western and Eastern blocks (Wang et al., 2010, 2014). In addition, the mafic dikes in the Lvliang area possibly represent the products of the subduction initiation (Wang et al., 2014). In summary, we propose a modified Paleoproterozoic tectonic model for the ZTM region (Fig. 14). At ~1900 Ma, A back-arc basin may have been formed along the western margin of the Eastern Block. The lithospheric mantle beneath the back-arc basin may have been metasomatized by reduced subduction-related fluids. Partial melting of the metasomatized mantle source may have generated the Paleoproterozoic ZTM Fe-rich mafic sills.

The Paleoproterozoic (2000–1800 Ma) is widely regarded to be a period of subduction, collision and extension for the TNCO (e.g., Wang et al., 2004, 2007, 2008, 2014; Zhai et al., 2005; Peng et al., 2006, 2013; Zhao et al., 2008). Previously, discussions on the final collision timing between the Eastern- and Western blocks have been focused mainly on the U-Pb ages of the metamorphic- and detrital zircons from the TNCO (e.g., Guan et al., 2002; Zhao et al., 2002, 2008; Kröner et al., 2006; Zhang et al., 2009; Li et al., 2011; Liu et al., 2011a,b, 2012). In this study, we have offered a new perspective to the discussion by integrating geochemical evidence and zircon U-Pb dating of the TNCO igneous rocks, with the aim to provide more effective and direct constraints on the final collision time. As a key area of the TNCO geological research, the ZTM has experienced long and complex tectonic evolution, especially in the Proterozoic (Sun et al., 1990; Sun and Hu, 1993; Bai et al., 1997). Two opposite hypotheses have been proposed for the possible tectonic setting of the ZTM at ~1900 Ma: (1) A major crustal reworking and thickening (Sun and Hu, 1993); (2) An active continental margin and a lateral growth of the crust (Liu et al., 2012 and references therein). Our results have shown that the formation of the ZTM Fe-rich mafic sills was subduction-related, which reflects a lateral growth of the crust at ~1900 Ma at the ZTM. The final collision between the Western- and Eastern blocks may have taken place no earlier than 1900 Ma, which is consistent with the widely accepted ~1850 Ma collision model (Zhao et al., 2001, 2005; Zhai et al., 2010).

As discussed before, there are also two models for the ~1850 Ma Ga collision: (1) A continuous subduction since 2500 Ma between the Western- and Eastern blocks until their final collision (Zhao et al., 2001, 2005; Liu et al., 2011a,b, 2012, 2014) and (2) Amalgamation of some micro-blocks at ~2500 Ma Ga, followed by another rifting-subduction-collision cycle in the Proterozoic (Zhai et al., 2010; Zhai and Santosh, 2013). The rifting events, occurred at ~2100 Ma, are evidenced by the presence of bimodal volcanic rocks

(Sun and Hu, 1993; Zhai and Santosh, 2013). In fact, the ~2100 Ma rift-related igneous rocks are widespread in the TNCO, for example, the ~2100 Ma mafic dikes at Lvliang (Wang et al., 2014), the ~2100 Ma quartz-monzonite porphyry in the ZTM (Li et al., 2013b) and the ~2100 Ma A1-type granite at Wutai (Eby, 1992; Du et al., 2013). In addition, the majority of detrital zircon U-Pb ages from the Lower Zhongtiao Subgroup and Jiangxian Group, both of them deposited between 2200 and 2100 Ma, are significantly older than the deposition age of the rocks (Li et al., 2008, 2011; Liu et al., 2012), which may reflect a passive margin environment (Cawood et al., 2012). Furthermore, the rate of crustal growth have been reduced at ~2100 Ma (Zhai and Santosh, 2013), which was also consistent with a passive margin setting. To conclude, our new evidence supports the second model proposed by Zhai et al. (2010).

6. Conclusions

The Fe-rich mafic sills in the ZTM (southern TNCO), characterized by the Nb-Ta and Ti depletions, are indicative of arc magmatism in an active continental margin setting. The Fe-rich mafic magma has been fractionated from a parental magma derived from the partial melting of a spinel lherzolite mantle source, which may have been metasomatized by reduced high-Fe subduction-related fluids. The petrogenesis of ZTM Fe-rich mafic sills was influenced by the combination of Fe enrichment mantle source and low fO_2 during magmatic evolution. These Fe-rich mafic sills were likely to have formed in a back-arc basin setting at ~1900 Ma, suggesting that the final collision between Western- and Eastern Blocks of the NCC should have occurred after 1900 Ma.

Acknowledgments

We would like to thank G.-Q. Hu, Y. Liu, J.-L. Ma and H. Zhang for their help during the geochemical and geochronological analyses. Two anonymous reviewers are gratefully acknowledged for their comments and suggestions that greatly enhance the manuscript. We thank the guest editor Y.-S. Wan for her insightful comments. This research is financially supported by the National Basic Research Program of China (Grant No. 2012CB416603). This is contribution No. IS-1952 from GIGCAS.

References

- Aldanmaz, E., Pearce, J.A., Thirlwall, M.F., Mitchell, J.G., 2000. Petrogenetic evolution of late Cenozoic, post-collision volcanism in western Anatolia, Turkey. *J. Volcanol. Geotherm. Res.* 102, 67–95.
- Arndt, N., Lehert, K., Vasil'ev, Y., 1995. Meimechites: highly magnesian lithosphere-contaminated alkaline magmas from deep subcontinental mantle. *Lithos* 34, 41–59.
- Ayers, J., 1998. Trace element modeling of aqueous fluid – peridotite interaction in the mantle wedge of subduction zones. *Contrib. Mineral. Petrol.* 132, 390–404.
- Bai, J., Yu, Z., Yan, Y., Dai, F., 1997. Precambrian Geology of Zhongtiaoshan. Tianjin Science and Technology Press, Tianjin, pp. 143 (in Chinese).
- Baker, J.A., Krogh Jensen, K., 2004. Coupled ^{186}Os – ^{187}Os enrichments in the earth's mantle–core–mantle interaction or recycling of ferromanganese crusts and nodules? *Earth Planet. Sci. Lett.* 220, 277–286.
- Bali, E., Audet, A., Keppler, H., 2011. The mobility of U and Th in subduction zone fluids: an indicator of oxygen fugacity and fluid salinity. *Contrib. Mineral. Petrol.* 161, 597–613.
- Brooks, C.K., Larsen, L.M., Nielsen, T.F.D., 1991. Importance of iron-rich tholeiitic magmas at divergent plate margins – a reappraisal. *Geology* 19, 269–272.
- Cawood, P., Hawkesworth, C., Dhuime, B., 2012. Detrital zircon record and tectonic setting. *Geology* 40, 875–878.
- Chauvel, C., Marini, J.C., Plank, T., Ludden, J.N., 2009. Hf-Nd input flux in the Izu–Mariana subduction zone and recycling of subducted material in the mantle. *Geochem. Geophys. Geosyst.* 10, Q01001.
- Class, C., Miller, D.M., Goldstein, S.L., Langmuir, C.H., 2000. Distinguishing melt and fluid subduction components in Umnak Volcanics, Aleutian Arc. *Geochem. Geophys. Geosyst.* 1, 1004.
- Coltorti, M., Bonadiman, C., Faccini, B., Grégoire, M., O'Reilly, S.Y., Powell, W., 2007. Amphiboles from suprasubduction and intraplate lithospheric mantle. *Lithos* 99, 68–84.
- Dobosi, G., Kempton, P.D., Downes, H., Embey-Isztin, A., Thirlwall, M., Greenwood, P., 2003. Lower crustal granulite xenoliths from the Pannonian Basin, Hungary, Part 2: Sr-Nd-Pb-Hf and O isotope evidence for formation of continental lower crust by tectonic emplacement of oceanic crust. *Contrib. Mineral. Petrol.* 144, 671–683.
- Du, L.L., Yang, C.H., Wang, W., Ren, L.D., Wan, Y.S., Wu, J.S., Zhao, L., Song, H.X., Geng, Y.S., Hou, K.J., 2013. Paleoproterozoic rifting of the North China Craton: geochemical and zircon Hf isotopic evidence from the 2137 Ma Huangjianshan A-type granite porphyry in the Wutai area. *J. Asian Earth Sci.* 72, 190–202.
- Eby, G.N., 1992. Chemical subdivision of the A-type granitoids: petrogenetic and tectonic implications. *Geology* 20, 641–644.
- Elliott, T., Plank, T., Zindler, A., White, W., Bourdon, B., 1997. Element transport from slab to volcanic front at the Mariana arc. *J. Geophys. Res.* 102, 14991–15019.
- Erkul, S.T., Erkul, F., 2012. Magma interaction processes in syn-extensional granitoids: the Tertiary Menderes Metamorphic Core Complex, western Turkey. *Lithos* 142, 16–33.
- Esawi, E.K., 2004. AMPH-CLASS: an Excel spreadsheet for the classification and nomenclature of amphiboles based on the 1997 recommendations of the International Mineralogical Association. *Comput. Geosci.* 30, 753–760.
- Faure, M., Trap, P., Lin, W., Monié, P., Bruguier, O., 2007. Polyorogenic evolution of the Paleoproterozoic Trans-North China Belt, new insights from the in Lüliangshan–Hengshan–Wutaishan and Fuping massifs. *Episodes* 30, 95–106.
- Floyd, P.A., Kelling, G., Gokcen, S.I., Gokcen, N., 1991. Geochemistry and tectonic environment of basaltic rocks from the Misis Ophiolitic Melange, South Turkey. *Chem. Geol.* 89, 263–279.
- Gamble, J., Wright, I., Woodhead, J., McCulloch, M., 1994. Arc and back-arc geochemistry in the southern Kermadec arc–Ngatoro Basin and offshore Taupo Volcanic Zone, SW Pacific. *Geol. Soc. Lond. Spec. Publ.* 81, 193–212.
- Gasparik, T., Litvin, Y.A., 2002. Experimental investigation of the effect of metasomatism by carbonatic melt on the composition and structure of the deep mantle. *Lithos* 60, 129–143.
- Gibson, S.A., 2002. Major element heterogeneity in Archean to recent mantle plume starting-heads. *Earth Planet. Sci. Lett.* 195, 59–74.
- Gibson, S.A., Thompson, R.N., Dickin, A.P., 2000. Ferropicrites: geochemical evidence for Fe-rich streaks in upwelling mantle plumes. *Earth Planet. Sci. Lett.* 174, 355–374.
- Green, N.L., 2006. Influence of slab thermal structure on basalt source regions and melting conditions: REE and HFSE constraints from the Garibaldi volcanic belt, northern Cascadia subduction system. *Lithos* 87, 23–49.
- Gribble, R.F., Stern, R.J., Bloomer, S.H., Stüben, D., O'Hearn, T., Newman, S., 1996. MORB mantle and subduction components interact to generate basalts in the southern Mariana Trough back-arc basin. *Geochim. Cosmochim. Acta* 60, 2153–2166.
- Guan, H., Sun, M., Wilde, S.A., Zhou, X., Zhai, M., 2002. SHRIMP U-Pb zircon geochronology of the Fuping Complex: implications for formation and assembly of the North China Craton. *Precambrian Res.* 113, 1–18.
- Guo, L.S., Liu, S.W., Liu, Y.L., Tian, W., Xu, S.Q., Li, Q.G., Lv, Y.J., 2008. Zircon Hf isotopic features of TTG gneisses and formation environment of Precambrian Sushui Complex in Zhongtiao Mountains. *Acta Petrol. Sin.* 24, 140–148 (in Chinese with English abstract).
- Halls, H.C., Li, J., Davis, D., Hou, G., Zhang, B., Qian, X., 2000. A precisely dated Proterozoic palaeomagnetic pole from the North China craton, and its relevance to palaeocontinental reconstruction. *Geophys. J. Int.* 143, 185–203.
- Hammouda, T., 2003. High-pressure melting of carbonated eclogite and experimental constraints on carbon recycling and storage in the mantle. *Earth Planet. Sci. Lett.* 214, 357–368.
- Hawkesworth, C., Hergt, J., Ellam, R., McDermott, F., 1991. Element fluxes associated with subduction related magmatism. *Philos. Trans. R. Soc. Lond. A: Phys. Eng. Sci.* 335, 393–405.
- Hirose, K., Kushiro, I., 1993. Partial melting of dry peridotites at high pressures: determination of compositions of melts segregated from peridotite using aggregates of diamond. *Earth Planet. Sci. Lett.* 114, 477–489.
- Hollings, P., Smyk, M., Heaman, L.M., Halls, H., 2010. The geochemistry, geochronology and paleomagnetism of dikes and sills associated with the Mesoproterozoic Midcontinent Rift near Thunder Bay, Ontario, Canada. *Precambrian Res.* 183, 553–571.
- Hollings, P., Smyk, M., Cousens, B., 2012. The radiogenic isotope characteristics of dikes and sills associated with the Mesoproterozoic Midcontinent Rift near Thunder Bay, Ontario, Canada. *Precambrian Res.* 214, 269–279.
- Ichiyama, Y., Ishiwatari, A., 2005. HfSE-rich picritic rocks from the Mino accretionary complex, southwestern Japan. *Contrib. Mineral. Petrol.* 149, 373–387.
- Ichiyama, Y., Ishiwatari, A., Hirahara, Y., Shuto, K., 2006. Geochemical and isotopic constraints on the genesis of the Permian ferropicritic rocks from the Mino-Tamba belt, SW Japan. *Lithos* 89, 47–65.
- Ilnicki, S., Szczepański, J., Pin, C., 2013. From back-arc to rifted margin: geochemical and Nd isotopic records in Neoproterozoic? – Cambrian metabasites of the Bystrzyckie and Orlickie Mountains (Sudetes, SW Poland). *Gondwana Res.* 23, 1104–1121.
- Jang, Y.D., Naslund, H.R., McBirney, A.R., 2001. The differentiation trend of the Skaergaard intrusion and the timing of magnetite crystallization: iron enrichment revisited. *Earth Planet. Sci. Lett.* 189, 189–196.
- Jensen, L.S., 1976. A new cation plot for classifying subalkaline volcanic rocks. *Nat. Resour. Misc.* 66, 22.

- Jiang, C., Jia, C., Li, L., Zhang, P., Lu, D., Bai, K., 2004. Source of the Fe-riched-type high-Mg magma in Mazhartag region, Xinjiang. *Acta Geol. Sin.* 78, 770–780 (in Chinese with English abstract).
- Jiang, Y.H., Jiang, S.Y., Dai, B.Z., Liao, S.Y., Zhao, K.D., Ling, H.F., 2009. Middle to Late Jurassic felsic and mafic magmatism in southern Hunan province, southeast China: implications for a continental arc to rifting. *Lithos* 107, 185–204.
- Jiang, Y., Niu, H., Bao, Z., Li, N., Shan, Q., Yang, W., 2014. Fluid evolution of the Tongkuangyu porphyry copper deposit in the Zhongtiaoshan region: evidence from fluid inclusions. *Ore Geol. Rev.* 63, 498–509.
- Jochum, K., Arndt, N., Hofmann, A., 1991. Nb–Th–La in komatiites and basalts: constraints on komatiite petrogenesis and mantle evolution. *Earth Planet. Sci. Lett.* 107, 272–289.
- Keller, R.A., Fisk, M.R., Smellie, J.L., Strelkin, J.A., Lawver, L.A., 2002. Geochemistry of back arc basin volcanism in Bransfield Strait, Antarctica: subducted contributions and along-axis variations. *J. Geophys. Res.* 107, 2171.
- Kelley, K.A., Cottrell, E., 2009. Water and the oxidation state of subduction zone magmas. *Science* 325, 605–607.
- Kerrick, R., Polat, A., Wyman, D., Hollings, P., 1999. Trace element systematics of Mg-, to Fe-tholeiitic basalt suites of the Superior Province: implications for Archean mantle reservoirs and greenstone belt genesis. *Lithos* 46, 163–187.
- Kerrick, R., Polat, A., Xie, Q.L., 2008. Geochemical systematics of 2.7 Ga Kinojevis Group (Abitibi), and Manitouwadge and Winston Lake (Wawa) Fe-rich basalt–rhyolite associations: backarc rift oceanic crust? *Lithos* 101, 1–23.
- Kogarko, L.N., Kurat, G., Ntaflos, T., 2001. Carbonate metasomatism of the oceanic mantle beneath Fernando de Noronha Island, Brazil. *Contrib. Mineral. Petrol.* 140, 577–587.
- Kogiso, T., Hirose, K., Takahashi, E., 1998. Melting experiments on homogeneous mixtures of peridotite and basalt: application to the genesis of ocean island basalts. *Earth Planet. Sci. Lett.* 162, 45–61.
- Kröner, A., Wilde, S., Li, J., Wang, K., 2005. Age and evolution of a late Archean to Paleoproterozoic upper to lower crustal section in the Wutaishan/Hengshan/Fuping terrain of northern China. *J. Asian Earth Sci.* 24, 577–595.
- Kröner, A., Wilde, S., Zhao, G., O'Brien, P., Sun, M., Liu, D., Wan, Y., Liu, S., Guo, J., 2006. Zircon geochronology and metamorphic evolution of mafic dykes in the Hengshan Complex of northern China: evidence for late Paleoproterozoic extension and subsequent high-pressure metamorphism in the North China Craton. *Precambrian Res.* 146, 45–67.
- Kusky, T.M., 2011. Geophysical and geological tests of tectonic models of the North China Craton. *Gondwana Res.* 20, 26–35.
- Kusky, T.M., Li, J., 2003. Paleoproterozoic tectonic evolution of the North China Craton. *J. Asian Earth Sci.* 22, 383–397.
- Kusky, T., Li, J., Santosh, M., 2007a. The Paleoproterozoic north Hebei orogen: North China craton's collisional suture with the Columbia supercontinent. *Gondwana Res.* 12, 4–28.
- Kusky, T., Windley, B., Zhai, M.-G., 2007b. Tectonic evolution of the North China Block: from orogen to craton to orogen. *Geol. Soc. Lond. Spec. Publ.* 280, 1–34.
- La Flèche, M., Camire, G., Jenner, G., 1998. Geochemistry of post-Acadian, Carboniferous continental intraplate basalts from the Maritimes Basin, Magdalen Islands, Quebec, Canada. *Chem. Geol.* 148, 115–136.
- Lassiter, J.C., DePaolo, D.J., 1997. Plume/lithosphere interaction in the generation of continental and oceanic flood basalts: chemical and isotopic constraints. In: Mahoney, J.J., Coffin, M.F. (Eds.), Large Igneous Provinces, Continental, Oceanic and Planetary Flood Volcanism, vol. 100. Geophysical Monograph, American Geophysical Union, pp. 335–355.
- Leake, B.E., Woolley, A.R., Arps, C.E.S., Birch, W.D., Gilbert, M.C., Grice, J.D., Hawthorne, F.C., Kato, A., Kisch, H.J., Krivovichev, V.G., Linthout, K., Laird, J., Mandarino, J.A., Maresch, W.V., Nickel, E.H., Rock, N.M.S., Schumacher, J.C., Smith, D.C., Stephenson, N.C.N., Ungaretti, L., Whittaker, E.J.W., Guo, Y.Z., 1997. Nomenclature of amphiboles: report of the subcommittee on amphiboles of the International Mineralogical Association, Commission on New Minerals and Mineral Names. *Can. Mineral.* 35, 219–246.
- Leroex, A.P., Dick, H.J.B., Reid, A.M., Erlank, A.J., 1982. Ferrobasalts from the Spiess Ridge Segment of the Southwest Indian Ridge. *Earth Planet. Sci. Lett.* 60, 437–451.
- Leybourne, M.I., Van Wagoner, N., Ayres, L.D., 1999. Partial melting of a refractory subducted slab in a Paleoproterozoic island arc: implications for global chemical cycles. *Geology* 27, 731–734.
- Li, X.H., 1997. Geochemistry of the Longsheng Ophiolite from the southern margin of Yangtze Craton, SE China. *Geochim. J. Jpn.* 31, 323–338.
- Li, X., Qi, C., Liu, Y., Liang, X., Tu, X., Xie, L., Yang, Y., 2005a. Petrogenesis of the Neoproterozoic bimodal volcanic rocks along the western margin of the Yangtze Block: new constraints from Hf isotopes and Fe/Mn ratios. *Chin. Sci. Bull.* 50, 2481–2486.
- Li, X., Qi, C., Liu, Y., Liang, X., Tu, X., Xie, L., Yang, Y., 2005b. Rapid separation of Hf from rock samples for isotope analysis by MC-ICPMS: a modified single-column extraction chromatography method. *Geochimica* 34, 109–114 (in Chinese with English abstract).
- Li, X.-H., Li, Z.-X., Wingate, M.T., Chung, S.-L., Liu, Y., Lin, G.-C., Li, W.-X., 2006. Geochemistry of the 755 Ma Mundine Well dyke swarm, northwestern Australia: part of a Neoproterozoic mantle superplume beneath Rodinia? *Precambrian Res.* 146, 1–15.
- Li, Q.G., Liu, S.W., Wang, Z.Q., Zhang, F., Chen, Y.Z., Wang, T., 2008. LA-ICP-MS U-Pb geochronology of the detrital zircons from Jiangxian Group in the Zhongtiao Mountain and its tectonic significance. *Acta Petrol. Sin.* 24, 1359–1368 (in Chinese with English abstract).
- Li, Q., Chen, X., Liu, S., Wang, Z., Zhou, Y., Zhang, J., Wang, T., 2009. Evaluating the provenance of metasedimentary rocks of the Jiangxian Group from the Zhongtiao Mountain using whole-rock geochemistry and detrital zircon Hf isotope. *Acta Geol. Sin. Engl. Ed.* 83, 550–561.
- Li, Q., Liu, S., Wang, Z., Shen, Y., Zhang, L., Zhang, J., 2011. Provenance and geotectonic setting of the Paleoproterozoic Zhongtiao Group and implications for assembly of the North China Craton: whole-rock geochemistry and detrital zircon data. *J. Geol. Soc.* 168, 1215–1224.
- Li, J.L., Gao, J., John, T., Klemd, R., Su, W., 2013a. Fluid-mediated metal transport in subduction zones and its link to arc-related giant ore deposits: constraints from a sulfide-bearing HP vein in lawsonite eclogite (Tianshan, China). *Geochim. Cosmochim. Acta* 120, 326–362.
- Li, N.B., Lou, Y., Guo, S.L., Jiang, Y.H., Zeng, L.J., Niu, H.C., 2013b. Zircon U–Pb geochronology and Hf isotope geochemistry of metamorphic quartz–monzonite porphyry from Tongkuangyu area, Zhongtiao Mountain and its geological implications. *Acta Petrol. Sin.* 29, 2416–2424 (in Chinese with English abstract).
- Liang, X.R., Wei, G.J., Li, X.H., Liu, Y., 2003. Precise measurement of $^{143}\text{Nd}/^{144}\text{Nd}$ and Sm/Nd ratios using multiple-collectors inductively coupled plasma-mass spectrometer (MC-ICPMS). *Geochimica* 32, 91–96 (in Chinese with English abstract).
- Ling, M.X., Liu, Y.L., Williams, I.S., Teng, F.Z., Yang, X.Y., Ding, X., Wei, G.J., Xie, L.H., Deng, W.F., Sun, W.D., 2013. Formation of the world's largest REE deposit through protracted fluxing of carbonatite by subduction-derived fluids. *Sci. Rep.* 3, 1776.
- Liu, D., Nutman, A., Compston, W., Wu, J., Shen, Q.H., 1992. Remnants of ≥ 3800 Ma crust in the Chinese part of the Sino-Korean craton. *Geology* 20, 339–342.
- Liu, D.Y., Wan, Y., Wu, J., Wilde, S., Zhou, H., Dong, C., Yin, X., 2007. Eoarchean rocks and zircons in the North China Craton. *Dev. Precambrian Geol.* 15, 251–273.
- Liu, D., Wilde, S.A., Wan, Y., Wu, J., Zhou, H., Dong, C., Yin, X., 2008. New U–Pb and Hf isotopic data confirm Anshan as the oldest preserved segment of the North China Craton. *Am. J. Sci.* 308, 200–231.
- Liu, C., Zhao, G., Sun, M., Wu, F., Yang, J., Yin, C., Leung, W.H., 2011a. U–Pb and Hf isotopic study of detrital zircons from the Yejishan Group of the Lüliang Complex: constraints on the timing of collision between the Eastern and Western Blocks, North China Craton. *Sediment. Geol.* 236, 129–140.
- Liu, C., Zhao, G., Sun, M., Zhang, J., He, Y., Yin, C., Wu, F., Yang, J., 2011b. U–Pb and Hf isotopic study of detrital zircons from the Hutuo group in the Trans-North China Orogen and tectonic implications. *Gondwana Res.* 20, 106–121.
- Liu, C.H., Zhao, G.C., Sun, M., Zhang, J., Yin, C.Q., 2012. U–Pb geochronology and Hf isotope geochemistry of detrital zircons from the Zhongtiao Complex: constraints on the tectonic evolution of the Trans-North China Orogen. *Precambrian Res.* 222, 159–172.
- Liu, C., Zhao, G., Liu, F., Han, Y., 2014. Nd isotopic and geochemical constraints on the provenance and tectonic setting of the low-grade meta-sedimentary rocks from the Trans-North China Orogen, North China Craton. *J. Asian Earth Sci.* 94, 173–189.
- Ludwig, K., 2008. Isoplot 3.6: a geochronology toolkit for Microsoft Excel. Berkeley Geochronology Center, 77 pp.
- Mayer, B., Jung, S., Romer, R., Stracke, A., Haase, K., Garbe-Schönberg, C.-D., 2013. Petrogenesis of Tertiary hornblende-bearing lavas in the Rhön, Germany. *J. Petrol.* 54, 2095–2123.
- Mitchell, R.H., 1990. A review of the compositional variation of amphiboles in alkali plutonic complexes. *Lithos* 26, 135–156.
- Muecke, G., Pride, C., Sarkar, P., 1979. Rare earth element geochemistry of regional metamorphic rocks. *Phys. Chem. Earth* 11, 449–464.
- Peacock, S.M., 1990. Fluid processes in subduction zones. *Science* 248, 329–337.
- Pearce, J.A., Ernewein, M., Bloomer, S.H., Parson, L.M., Murton, B.J., Johnson, L.E., 1994. Geochemistry of Lau Basin volcanic rocks: influence of ridge segmentation and arc proximity. *Geol. Soc. Lond. Spec. Publ.* 81, 53–75.
- Peng, P., Zhai, M.G., Zhang, H.F., Guo, J.H., 2005. Geochronological constraints on the paleoproterozoic evolution of the North China craton: SHRIMP zircon ages of different types of mafic dikes. *Int. Geol. Rev.* 47, 492–508.
- Peng, P., Zhai, M., Guo, J., 2006. 1.80–1.75 Ga Mafic Dyke Swarms in the Central North China Craton: Implications for a Plume-Related Break-Up Event. Dyke Swarms-Time Markers of Crustal Evolution. Taylor & Francis, London, pp. 99–112.
- Peng, P., Zhai, M.G., Guo, J.H., Kusky, T., Zhao, T.P., 2007. Nature of mantle source contributions and crystal differentiation in the petrogenesis of the 1.78 Ga mafic dykes in the central North China craton. *Gondwana Res.* 12, 29–46.
- Peng, P., Bleeker, W., Ernst, R.E., Söderlund, U., McNicol, V., 2011. U–Pb baddeleyite ages, distribution and geochemistry of 925 Ma mafic dykes and 900 Ma sills in the North China craton: evidence for a Neoproterozoic mantle plume. *Lithos* 127, 210–221.
- Peng, T.P., Wilde, S.A., Fan, W.M., Peng, B.X., Mao, Y.S., 2013. Mesoproterozoic high Fe–Ti mafic magmatism in western Shandong, North China Craton: petrogenesis and implications for the final breakup of the Columbia supercontinent. *Precambrian Res.* 235, 190–207.
- Pe-Piper, G., 2007. Relationship of amphibole composition to host-rock geochemistry: the A-type gabbro-granite Wentworth pluton, Cobquid shear zone, eastern Canada. *Eur. J. Mineral.* 19, 29–38.
- Philippot, P., Selverstone, J., 1991. Trace-element-rich brines in eclogitic veins: implications for fluid composition and transport during subduction. *Contrib. Mineral. Petrol.* 106, 417–430.

- Plank, T., Langmuir, C.H., 1998. The chemical composition of subducting sediment and its consequences for the crust and mantle. *Chem. Geol.* 145, 325–394.
- Reubi, O., Sims, K.W.W., Bourdon, B., 2014. ^{238}U – ^{230}Th equilibrium in arc magmas and implications for the time scales of mantle metasomatism. *Earth Planet. Sci. Lett.* 391, 146–158.
- Rowe, M.C., Kent, A.J.R., Nielsen, R.L., 2009. Subduction influence on oxygen fugacity and trace and volatile elements in basalts across the Cascade Volcanic Arc. *J. Petrol.* 50, 61–91.
- Rudnick, R.L., Fountain, D.M., 1995. Nature and composition of the continental crust: a lower crustal perspective. *Rev. Geophys.* 33, 267–309.
- Rudnick, R., Gao, S., 2003. Composition of the continental crust. *Treatise Geochem.* 3, 1–64.
- Rutherford, L., Barovich, K., Hand, M., Foden, J., 2006. Continental ca. 1.7–1.69 Ga Fe-rich metatholeiites in the Curnamona Province, Australia: a record of melting of a heterogeneous, subduction-modified lithospheric mantle. *Aust. J. Earth Sci.* 53, 501–519.
- Santosh, M., 2010. Assembling North China Craton within the Columbia supercontinent: the role of double-sided subduction. *Precambrian Res.* 178, 149–167.
- Sheraton, J., 1984. Chemical changes associated with high-grade metamorphism of mafic rocks in the East Antarctic Shield. *Chem. Geol.* 47, 135–157.
- Shervais, J.W., 1982. Ti–V plots and the petrogenesis of modern and ophiolitic lavas. *Earth Planet. Sci. Lett.* 59, 101–118.
- Skovgaard, A.C., Storey, M., Baker, J., Blusztajn, J., Hart, S.R., 2001. Osmium–oxygen isotopic evidence for a recycled and strongly depleted component in the Iceland mantle plume. *Earth Planet. Sci. Lett.* 194, 259–275.
- Sobolev, A.V., Hofmann, A.W., Kuzmin, D.V., Yaxley, G.M., Arndt, N.T., Chung, S.L., Danyushevsky, L.V., Elliott, T., Frey, F.A., Garcia, M.O., Gurenko, A.A., Kamenetsky, V.S., Kerr, A.C., Krivolutskaya, N.A., Matviienko, V.V., Nikogosian, I.K., Rocholl, A., Sigurdsson, I.A., Sushchanskaya, N.M., Teklay, M., 2007. The amount of recycled crust in sources of mantle-derived melts. *Science* 316, 412–417.
- Song, B., Nutman, A.P., Liu, D.Y., Wu, J.S., 1996. 3800–2500 Ma crustal evolution in the Anshan area of Liaoning Province, northeastern China. *Precambrian Res.* 78, 79–94.
- Sun, D.Z., Hu, W.X., 1993. *Precambrian Chronotectonic Framework and Model of Chronocrustal Structure of the Zhongtiao Mountains*. Geology Publishing House, Beijing, pp. 108–117 (in Chinese).
- Sun, S.S., McDonough, W., 1989. Chemical and isotopic systematics of oceanic basalts: implications for mantle composition and processes. *Geol. Soc. Lond. Spec. Publ.* 42, 313–345.
- Sun, D., Hu, W., Tang, M., Zhao, F., Condie, K.C., 1990. Origin of Late Archean and Early Proterozoic rocks and associated mineral deposits from the Zhongtiao Mountains, east-central China. *Precambrian Res.* 47, 287–306.
- Tang, Y.J., Zhang, H.F., Nakamura, E., Ying, J.F., 2011. Multistage melt/fluid–peridotite interactions in the refertilized lithospheric mantle beneath the North China Craton: constraints from the Li–Sr–Nd isotopic disequilibrium between minerals of peridotite xenoliths. *Contrib. Mineral. Petrol.* 161, 845–861.
- Temizel, İ., Arslan, M., Ruffet, G., Peucat, J.J., 2012. Petrochemistry, geochronology and Sr–Nd isotopic systematics of the Tertiary collisional and post-collisional volcanic rocks from the Ulubey (Ordu) area, eastern Pontide, NE Turkey: implications for extension-related origin and mantle source characteristics. *Lithos* 128, 126–147.
- Trap, P., Faure, M., Lin, W., Monié, P., 2007. Late Paleoproterozoic (1900–1800 Ma) nappe stacking and polyphase deformation in the Hengshan–Wutaishan area: implications for the understanding of the Trans-North-China Belt, North China Craton. *Precambrian Res.* 156, 85–106.
- Trap, P., Faure, M., Lin, W., Bruguier, O., Monié, P., 2008. Contrasted tectonic styles for the Paleoproterozoic evolution of the North China Craton. Evidence for a ~2.1 Ga thermal and tectonic event in the Fuping Massif. *J. Struct. Geol.* 30, 1109–1125.
- Vervoort, J.D., Patchett, P.J., Blichert-Toft, J., Albarède, F., 1999. Relationships between Lu–Hf and Sm–Nd isotopic systems in the global sedimentary system. *Earth Planet. Sci. Lett.* 168, 79–99.
- Wan, Y.S., Liu, D.Y., Wang, W., Song, T.R., Kröner, A., Dong, C.Y., Zhou, H.Y., Yin, X.Y., 2011. Provenance of Meso- to Neoproterozoic cover sediments at the Ming Tombs, Beijing, North China Craton: an integrated study of U–Pb dating and Hf isotopic measurement of detrital zircons and whole-rock geochemistry. *Gondwana Res.* 20, 219–242.
- Wan, Y.S., Liu, D.Y., Nutman, A., Zhou, H.Y., Dong, C.Y., Yin, X.Y., Ma, M.Z., 2012. Multiple 3.8–3.1 Ga tectono-magmatic events in a newly discovered area of ancient rocks (the Shengousi Complex), Anshan, North China Craton. *J. Asian Earth Sci.* 54–55, 18–30.
- Wang, Y., Fan, W., Zhang, Y., Guo, F., 2003. Structural evolution and $^{40}\text{Ar}/^{39}\text{Ar}$ dating of the Zanhuang metamorphic domain in the North China Craton: constraints on Paleoproterozoic tectonothermal overprinting. *Precambrian Res.* 122, 159–182.
- Wang, Y.J., Fang, W.M., Zhang, Y.H., Guo, F., Zhang, H.F., Peng, T.P., 2004. Geochemical Ar–40/Ar–39 geochronological and Sr–Nd isotopic constraints on the origin of Paleoproterozoic mafic dikes from the southern Taihang Mountains and implications for the ca. 1800 Ma event of the North China Craton. *Precambrian Res.* 135, 55–77.
- Wang, Y.J., Zhao, G.C., Fan, W.M., Peng, T.P., Sun, L.H., Xia, X.P., 2007. LA–ICP–MS U–Pb zircon geochronology and geochemistry of Paleoproterozoic mafic dykes from western Shandong Province: implications for back-arc basin magmatism in the Eastern Block, North China Craton. *Precambrian Res.* 154, 107–124.
- Wang, Y., Zhao, G., Cawood, P.A., Fan, W., Peng, T., Sun, L., 2008. Geochemistry of Paleoproterozoic (~1770 Ma) mafic dikes from the Trans-North China Orogen and tectonic implications. *J. Asian Earth Sci.* 33, 61–77.
- Wang, R.C., Che, X.D., Zhang, W.L., Zhang, A.C., Zhang, H., 2009. Geochemical evolution and late re-equilibration of Na–Cs-rich beryl from the Koktokay #3 pegmatite (Altai, NW China). *Eur. J. Mineral.* 21, 795–809.
- Wang, J., Wu, Y.B., Gao, S., Peng, M., Liu, X.C., Zhao, L.S., Zhou, L., Hu, Z.C., Gong, H.J., Liu, Y.S., 2010. Zircon U–Pb and trace element data from rocks of the Huai'an Complex: new insights into the late Paleoproterozoic collision between the Eastern and Western Blocks of the North China Craton. *Precambrian Res.* 178, 59–71.
- Wang, X., Zhu, W., Ge, R., Luo, M., Zhu, X., Zhang, Q., Wang, L., Ren, X., 2014. Two episodes of Paleoproterozoic metamorphosed mafic dykes in the Lvliang Complex: implications for the evolution of the Trans-North China Orogen. *Precambrian Res.* 243, 133–148.
- Weaver, B.L., Tarney, J., 1981. Chemical changes during dyke metamorphism in high-grade basement terrains. *Nature* 289, 47–49.
- Wiedenbeck, M., Allé, P., Corfu, F., Griffin, W.L., Meier, M., Oberli, F., Quadt, A.V., Roddick, J.C., Spiegel, W., 1995. Three natural zircon standards for U–Tu–Pb, Lu–Hf, trace element and REE analyses. *Geostand. Newsl.* 19, 1–23.
- Wilde, S.A., Zhao, G.C., 2005. Archean to Paleoproterozoic evolution of the North China Craton. *J. Asian Earth Sci.* 24, 519–522.
- Winchester, J., Floyd, P., 1977. Geochemical discrimination of different magma series and their differentiation products using immobile elements. *Chem. Geol.* 20, 325–343.
- Woodhead, J., Eggins, S., Gamble, J., 1993. High field strength and transition element systematics in island arc and back-arc basin basalts: evidence for multi-phase melt extraction and a depleted mantle wedge. *Earth Planet. Sci. Lett.* 114, 491–504.
- Xu, Y., Mei, H., Xu, J., Huang, X., Wang, Y., Chung, S.-L., 2003. Origin of two differentiation trends in the Emeishan flood basalts. *Chin. Sci. Bull.* 48, 390–394.
- Yang, W.B., Niu, H.C., Shan, Q., Luo, Y., Sun, W.D., Li, C.Y., Li, N.B., Yu, X.Y., 2012. Late Paleozoic calc-alkaline to shoshonitic magmatism and its geodynamic implications, Yuximolegal area, western Tianshan, Xinjiang. *Gondwana Res.* 22, 325–340.
- Yang, W.B., Niu, H.C., Shan, Q., Sun, W.D., Zhang, H., Li, N.B., Jiang, Y.H., Yu, X.Y., 2013. Geochemistry of magmatic and hydrothermal zircon from the highly evolved Baerzhe alkaline granite: implications for Zr–REE–Nb mineralization. *Mineralium Deposita*, 1–20.
- You, C.F., Castillo, P.R., Gieskes, J.M., Chan, L.H., Spivack, A.J., 1996. Trace element behavior in hydrothermal experiments: implications for fluid processes at shallow depths in subduction zones. *Earth Planet. Sci. Lett.* 140, 41–52.
- Yu, S., Liu, S., Tian, W., Li, Q., Feng, Y., 2006. SHRIMP zircon U–Pb chronology and geochemistry of the Henglingguan and Beiyu granitoids in the Zhongtiao Mountains, Shanxi Province. *Acta Geol. Sin. Engl. Ed.* 80, 912–924.
- Yuan, H., Gao, S., Liu, X., Li, H., Günther, D., Wu, F., 2004. Accurate U–Pb age and trace element determinations of zircon by laser ablation-inductively coupled plasma-mass spectrometry. *Geostand. Geanal. Res.* 28, 353–370.
- Zhai, M.G., 2010. Tectonic evolution and metallogenesis of North China Craton. *Min. Depos.* 29, 24–36 (in Chinese with English abstract).
- Zhai, M.G., Santosh, M., 2011. The early Precambrian odyssey of the North China Craton: a synoptic overview. *Gondwana Res.* 20, 6–25.
- Zhai, M.G., Santosh, M., 2013. Metallogenesis of the North China Craton: link with secular changes in the evolving Earth. *Gondwana Res.* 24, 275–297.
- Zhai, M.G., Guo, J.H., Liu, W.J., 2005. Neoproterozoic to Paleoproterozoic continental evolution and tectonic history of the North China Craton: a review. *J. Asian Earth Sci.* 24, 547–561.
- Zhai, M., Li, T.S., Peng, P., Hu, B., Liu, F., Zhang, Y., 2010. Precambrian key tectonic events and evolution of the North China Craton. *Geol. Soc. Lond. Spec. Publ.* 338, 235–262.
- Zhang, J., Zhao, G., Li, S., Sun, M., Wilde, S.A., Liu, S., Yin, C., 2009. Polyphase deformation of the Fuping Complex, Trans-North China Orogen: structures, SHRIMP U–Pb zircon ages and tectonic implications. *J. Struct. Geol.* 31, 177–193.
- Zhang, R.Y., Zhang, C.L., Diwu, C.R., Sun, Y., 2012a. Zircon U–Pb geochronology, geochemistry and its geological implications for the Precambrian granitoids in Zhongtiao Mountain, Shanxi Province. *Acta Petrol. Sin.* 28, 3559–3573 (in Chinese with English abstract).
- Zhang, Y.Z., Wang, Y.J., Fan, W.M., Zhang, A.M., Ma, L.Y., 2012b. Geochronological and geochemical constraints on the metasomatised source for the Neoproterozoic (similar to 825 Ma) high-mg volcanic rocks from the Cangshuiupu area (Hunan Province) along the Jiangnan domain and their tectonic implications. *Precambrian Res.* 220, 139–157.
- Zhang, R.Y., Zhang, C.L., Sun, Y., 2013a. Crustal reworking in the North China Craton at ~2.5 Ga: evidence from zircon U–Pb ages, Hf isotopes and whole-rock geochemistry of the TTG gneisses in the Zhongtiao Mountain. *Acta Petrol. Sin.* 29, 2265–2280 (in Chinese with English abstract).
- Zhang, Y.Z., Wang, Y.J., Geng, H.Y., Zhang, Y.H., Fan, W.M., Zhong, H., 2013b. Early Neoproterozoic (similar to 850 Ma) back-arc basin in the Central Jiangnan Orogen (Eastern South China): geochronological and petrogenetic constraints from meta-basalts. *Precambrian Res.* 231, 325–342.
- Zhao, G.C., Zhai, M.G., 2013. Lithotectonic elements of Precambrian basement in the North China Craton: review and tectonic implications. *Gondwana Res.* 23, 1207–1240.
- Zhao, G., Wilde, S.A., Cawood, P.A., Sun, M., 2001. Archean blocks and their boundaries in the North China Craton: lithological, geochemical, structural and P–T path constraints and tectonic evolution. *Precambrian Res.* 107, 45–73.
- Zhao, G., Wilde, S.A., Cawood, P.A., Sun, M., 2002. SHRIMP U–Pb zircon ages of the Fuping Complex: implications for late Archean to Paleoproterozoic accretion and assembly of the North China Craton. *Am. J. Sci.* 302, 191–226.

- Zhao, G., Sun, M., Wilde, S.A., Sanzhong, L., 2005. Late Archean to Paleoproterozoic evolution of the North China Craton: key issues revisited. *Precambrian Res.* 136, 177–202.
- Zhao, G., Wilde, S.A., Sun, M., Guo, J., Kröner, A., Li, S., Li, X., Zhang, J., 2008. SHRIMP U-Pb zircon geochronology of the Huai'an Complex: constraints on late Archean to Paleoproterozoic magmatic and metamorphic events in the Trans-North China Orogen. *Am. J. Sci.* 308, 270–303.
- Zhao, G., Yin, C., Guo, J., Sun, M., Li, S., Li, X., Wu, C., Liu, C., 2010. Metamorphism of the Lüliang amphibolite: implications for the tectonic evolution of the North China Craton. *Am. J. Sci.* 310, 1480–1502.
- Zhao, B., Wang, D.H., HOu, K.J., Liu, R.L., 2012. Isochronology study on Sushui Complex in Zhongtiao Mountains and its geological significance. *J. Earth Sci. Environ.* 34, 1–8.
- Zheng, T., Zhao, L., Zhu, R., 2009. New evidence from seismic imaging for subduction during assembly of the North China Craton. *Geology* 37, 395–398.
- Zhu, Y., Guo, X., Song, B., Zhang, L., Gu, L., 2009. Petrology, Sr-Nd-Hf isotopic geochemistry and zircon chronology of the Late Paleozoic volcanic rocks in the southwestern Tianshan Mountains, Xinjiang, NW China. *J. Geol. Soc.* 166, 1085–1099.
- Zhu, W.-G., Zhong, H., Li, X.-H., He, D.-F., Song, X.-Y., Ren, T., Chen, Z.-Q., Sun, H.-S., Liao, J.-Q., 2010. The early Jurassic mafic-ultramafic intrusion and A-type granite from northeastern Guangdong, SE China: age, origin, and tectonic significance. *Lithos* 119, 313–329.
- Zhu, X., Zhai, M., Chen, F., Lyu, B., Wang, W., Peng, P., Hu, B., 2013. ~2.7-Ga crustal growth in the North China Craton: evidence from zircon U-Pb ages and Hf isotopes of the Sushui Complex in the Zhongtiao Terrane. *J. Geol.* 121, 239–254.